Earth System
Science
Data

Open Access

Supplement of

Multi-year observations of BVOCs and ozone: concentrations and fluxes measured above and below the canopy in a mixed temperate forest

Clément Dumont et al.

Correspondence to: Clément Dumont (clement.dumont@uliege.be)

Contents

S1 Compounds and parameters measured at BE-Vie

Table S1: Overview of instruments and related measurements. The access to the four distinct datasets (groups *i*, *ii*, *iii* and *iv*) are given in Sect. *Code and data availability.*

Compound/ Parameter	Instrument (manufacturer)	Measurement principle	Acquisition frequency (aggregation frequency)	Variable type	Heights(s) [m a.g.l.]
(i) Main measurements (present study)					
VOC	PTR-ToF-4000 (Ionicon Analytik)	proton-transfer mass spectro.	10 Hz (35 min)	Conc. profile	3-11-19-27-35-43-51
			10 Hz (1 min/30 min)	Conc. & Flux	51
			10 Hz (1 min/30 min)	Conc. & Flux	3[a]
O_3	T400 (Teledyne)	UV absorption	6 s (35 min)	Conc. profile	3-11-19-27-35-43-51
			6 s (1 min/30 min)	Conc. & Flux	51
			6 s (1 min/30 min)	Conc. & Flux	3[a]
O_3	FOS (Sextant)	chemi-luminescence	10 Hz (30 min)	Flux	51
O_3	FOS (Sextant)	chemi-luminescence	10 Hz (30 min)	Flux	3
3D wind	HS-50 (Gill)	ultrasonic time-of-flight	10 Hz (30 min)	-	6-18-51
3D wind	R3 (Gill)	ultrasonic time-of-flight	10 Hz (30 min)	-	3-12-24-30-36
(ii) ICOS measurements					
Comprehensive set of meteorological and phenological variables					
A complete description of ICOS variables is available along with the downloaded dataset.					
(iii) ISSeP measurements					
VOC	Clarus 500 GC/MS + Turbo Matrix ATD (Perkin Elmer)	offline GC-MS	every 2 days (23h sampling)	Conc.	3
PAH	Agilent GC/MS (Agilent)	foam for offline GC-MS	15 days	Conc.	3
O_3	APOA-370 (Horiba)	UV absorption	10 s (30 min)	Conc.	4
NO	APNA-370 (Horiba)	chemi-luminescence	10 s (30 min)	Conc.	4
NO_2	APNA-370 (Horiba)	chemi-luminescence + MO-converter	10 s (30 min)	Conc.	4
CO	APMA-370 (Horiba)	non-dispersive IR photometry	10 s (30 min)	Conc.	4
SO_2	APSA-370 (Horiba)	UV fluorescence	10 s (30 min)	Conc.	4
Hg	2537X (Tekran)	cold vapour atomic fluorescence	10 s (30 min)	Conc.	4
PM2.5 + PM10	EDM180 (Grimm)	optical particle size spectrometer	10 s (30 min)	Conc.	3.5
PM2.5 + PM10[a,b]	APS 3321 (TSI)	aeorodynamical particle sizer	10 s (5 min)	Aerodyn. diameter	3.5
PM2.5 + PM10	SEQ47/50-RV-CD (Leckel)	gravimetry	24h	Conc.	1.5

Table S1 (continued)

Compound/ Parameter	Instrument (manufacturer)	Measurement principle	Acquisition frequency (aggregation frequency)	Variable type	Heights(s) [m a.g.l.]
Ultrafine particles	APS 3321 PM9 (Tropos)	scanning mobility + condensation particle sizer	5 min	Particle size distribution	3.5
Ultrafine particles	3750-10-CEN (TSI)	condensation particle sizer	10 s (5 min)	Particle number	3.5
BC	BC1054 (Met One)	aethalometer	5 min (30 min)	Particle light abs. coeff.	3.5
BC[a]	AE33 (Magee)	aethalometer	5 min	Particle light abs. coeff.	3.5
EC, OC	PNS 16T (Deenda) OCEC Model 4L (Sunset Lab)	thermal-optical analysis	24 h	Conc.	1.5
Aerosols	Aurora 3000 (Acoem)	nephtelometry	5 min	Particle light (back)scattering coeff.	3.5
(iv) Remote-sensing measurements					
HCHO +NO$_2$[c]	Skyspec Compact (Airyx)	multi-axis differential optical abs. spectroscopy	20 min	Column density Conc.	tropos. column + vertical profile
Aerosols[c]	Skyspec Compact (Airyx)	multi-axis differential optical abs. spectroscopy	20 min	Aerosol Optical depth	tropos. column + vertical profile

[a] Not available in 2022
[b] Not available in 2023
[c] Not available in 2024

S2 VOC concentrations

S2.1 PTR-ToF-MS data processing chain

Peak identification and integration of recorded spectra were performed on a near-daily basis with the Ionicon Data Analyzer software (IDA; 2022, v 1.0.0.2; 2023, v 2.0.1.2; 2024, v 2.2.1.1). Subsequent data processing was performed in a python-based framework referred to as the Peak Area Processing software (PAP) which was used for non-targeted peak selection, instrument characterization, and quantification of mixing ratios with related uncertainties at both 10 Hz and 1 min time resolution. Updated information on sensitivities, expanded uncertainty calculation, and data flagging were performed in a post-processing step to generate the final database.

S2.1.1 Mass selection

The mass scale was calibrated in the IDA software every 60 s and peak-shapes were considered stable over the course of 1 hour. Independent peak identification was performed for each IDA analysis with up to 8 m/z values identified per peak system (collection of isobaric peaks with the same nominal mass). A peak system was only considered for analysis if its maximum ion signal intensity exceeded 0.1 cps.

To obtain a list of non-targeted m/z ratios, Density-Based Spatial Clustering of Applications with Noise (Ester et al., 1996), or DBSCAN, was employed for each campaign using the PAP framework to identify mass-to-charge ratios where peaks were regularly observed. The DBSCAN clustering algorithm makes use of two parameters (ϵ: maximum difference between m/z values to be grouped; min_samples: number of elements in a group to be considered as a cluster). To optimize the choice of both parameters, we performed a scan of the ϵ-space for min_samples values of 10, 20, 30, 40% of the number of IDA analyses performed in the campaign. To evaluate the results of DBSCAN, we tried to minimize (i) the number of peaks identified by IDA not associated with a cluster, and (ii) the number of clusters with more than 1 peak associated in the same IDA file. The first is equivalent to reducing the amount of peaks identified as noise (i.e., peaks not associated to any cluster) as much as possible, while the second is a limit on how wide clusters are allowed to become without combining distinct peaks in the same peak system. The optimal ϵ value for a specific min_samples choice generally coincided with the maximum amount of clusters identified by DBSCAN.

An automated selection of the resulting m/z clusters has been performed based on (i) the width of the DBSCAN intervals centred around the mass (stability of peak identification by IDA), (ii) fraction of data above the limit of quantification (significance of concentrations), and (iii) m/z localization (interpretability of the data). Afterwards, a manual selection to discard m/z values related to isotopes or hydrated ion species was done. Compound attribution was performed by making use of PTR-MS databases (Pagonis et al., 2019; Yáñez-Serrano et al., 2021) and measurements reported at ecosystem sites (Kim et al., 2010; Hellén et al., 2018; Schallhart et al., 2018; Pfannerstill et al., 2021) to identify the compounds most likely to contribute to the observed signal (Table S3).

S2.1.2 Instrument characterization

Calibrations were performed every 3–4 days to characterize the instrument transmission and calculate calibration factors for compounds included in the calibration bottle (Table S2). Instrument transmission (relative to the one at m/z 21.022) was calculated using a subset of compounds (associated to m/z 33.033, 42.034, 45.033, 59.049, 79.054, 93.070, 107.086, and 180.937) included in the calibration bottle. The transmission curve between m/z 21.022 and 180.937 was defined through linear interpolation of transmissions obtained during calibrations. At high m/z, the transmission curve becomes more stable and we assumed a constant behaviour ($Tr_{mz>180.937} \equiv Tr_{180.937}$).

S2.1.3 Mixing ratio calculation

The mixing ratio of compounds was calculated using either the kinetic or the calibration approach, similar to the discussion in the ACTRIS measurement guidelines for VOC analysis with PTR-MS instruments (Dusanter S. et al., 2025). In both cases, integrated peak areas (cps) obtained from IDA were corrected for ion transmission, and normalized with respect to a source ion peak area of 10^6 counts per second (cps) to account for variations in the source ion production.

Transmission-corrected normalized peak areas I^*_{mz}, expressed in transmission-corrected normalized counts per second (tc-ncps), for the VOC-related ion species at mass-to-charge ratio m/z, are defined as follows:

$$I^*_{mz} = \frac{10^6}{488 \cdot I_{21.022} + 669 \cdot X_r \cdot Tr^{-1}_{38.033} \cdot I_{38.033}} \frac{I_{mz}}{Tr_{mz}}, \tag{S1}$$

Table S2: Concentrations and uncertainties (ppbv) of compounds included in the calibration standards (*Apel-Riemer Environmental Inc., FL, USA*) used during the measurement campaigns at BE-Vie. The first standard was replaced on site on Oct. 17, 2024. Compounds used to quantify instrument transmission are highlighted in bold. The uncertainty interval was provided by the manufacturer and is a result of the combined uncertainty due to gravimetric preparation, long-term response factor uncertainty, and the uncertainty in analysis with a coverage factor of 2.

Compound	Standard 1		Standard 2	
	Concentration	Uncertainty	Concentration	Uncertainty
Acetaldehyde	991	32	1006	36
Methanol	1030	48	1068	70
Ethanol	537	20	493	20
Acetonitrile	537	20	490	20
Acetone	1006	36	1026	33
Isoprene	499	16	508	15
Methacrolein	477	16	470	14
Methyl Vinyl Ketone	514	17	501	15
Methyl Ethyl Ketone	520	17	502	19
Benzene	514	17	506	15
cis-3-Hexenol	948	31	986	31
Toluene	494	16	491	15
1,2,4-Trifuorobenzene	536	27	531	22
m-Xylene	492	16	487	30
Sabinene	976	36	982	30
1,2,4-Trimethylbenzene	479	19	482	17
Octamethylcyclotetrasiloxane	987	37	989	32
Decamethylcyclopentasiloxane	979	48	1008	31
1,2,4-Trichlorobenzene	485	15	485	15

where I_{mz} and Tr_{mz} are the non-normalized peak area (cps) and the ion transmission at the specific m/z, respectively. The factors 488 and 669 in the denominator are the isotopic multiplication factors for H_3O^+ and $H_3O^+(H_2O)$ at m/z 21.022 and 38.033, respectively. It was suggested by de Gouw and Warneke (2007) to include a species-specific X_r factor in the denominator to account for humidity dependence in the ion signal. Here, X_r was set to 1, similar to the quantification procedure described by Simon et al. (2023).

The volume mixing ratio (VMR) was calculated by dividing the background-subtracted transmission-corrected normalized ion intensity by the compound-dependent sensitivities:

$$\text{VMR}_X = \frac{I_{mz}^*(\text{ambient}) - I_{mz}^*(\text{background})}{S_{X,mz}}, \tag{S2}$$

here, $S_{X,mz}$ denotes the sensitivity (tc-ncps ppbv^{-1}) for compound X measured at mass-to-charge ratio m/z. For compounds included in the calibration mixture, $S_{X,mz}$ was calculated at every calibration. For compounds not included in the gas standard, the kinetic approach was used and compound-specific sensitivities were calculated through:

$$S_{X,mz} = k_X \cdot FY_{X,mz} \cdot IF_{X,mz} \cdot N_{\text{DT}} \cdot \tau_{\text{reac}}, \tag{S3}$$

where k_X is the collision rate constant of X with H_3O^+, $FY_{X,mz}$ is the relative contribution (%) of the reaction channel (e.g. non-dissociative proton transfer, or dissociative proton transfer followed by ejection of a water ligand) leading to product ions with m/z = mz, $IF_{X,mz}$ is a multiplication factor for considering all isotopes of the m/z product ions associated with the reaction channel, and N_{DT} and τ_{reac} are the air number density and reaction time in the drift tube, respectively. The reaction time, which depends on the instrument configuration and operational conditions, is calculated by:

$$\tau_{\text{reac}} = \frac{d^2}{\mu_0 \cdot N_0} \frac{N_{\text{DT}}}{U}, \tag{S4}$$

where μ_0 is the reduced mobility of H_3O^+ in air (2.76 cm^2 V^{-1} s^{-1}), N_0 the gas number density at standard pressure and temperature, d the length of the drift tube (9.2 cm), and U the drift voltage.

Collision rate constants of the H_3O^+/VOC reaction were determined at the PTR-ToF-MS operational conditions, calculated by using parametrizations based on trajectory analysis (Su, 1994). Rate constants

are provided for those compounds for which polarizability and dipole moments were available. A standard rate constant of 2.5×10^{-9} cm^3 molecule^{-1} s^{-1} was used for compounds for which parameters were lacking for rate constant calculation, but for which proton transfer or fragment yields were available in the literature. For hydroxyacetone (m/z 75.0441), however, a collision rate constant of 3.5×10^{-9} cm^3 molecule^{-1} s^{-1} was used based on Karl et al. (2009). The collision rate constants and a full list of the sensitivities used can be found in Table S3.

S2.1.4   Uncertainty quantification

The integrated peak area obtained from the IDA software is determined by a combination of operations (peak shape determination, peak identification, and baseline subtraction (Müller et al., 2013)) for which no uncertainties are provided. To estimate a statistical uncertainty (precision) on the peak areas, we either assume the total number of counts associated to a measurement follows a Poisson distribution, or we combine a number of 100 ms measurements and considered them to be normally distributed during the accumulation interval. The ACTRIS measurement guideline (Dusanter S. et al., 2025) favours the Poisson assumption and the precision of the count rate ($\sigma_{I_{mz}}$) is calculated by:

$$\sigma_{I_{mz}} = \frac{\sqrt{I_{mz} \cdot \Delta t}}{\Delta t}, \tag{S5}$$

with Δt the measurement interval. This was used to calculate uncertainties on the 100 ms data. We highlight that as IDA performs a baseline subtraction before calculating the peak area, the Poisson assumption does not strictly hold. Moreover, the value of I_{mz} occasionally drops below zero and precision values are not quantifiable. When combining N measurements over longer intervals, we could consider the analyte to be at a constant concentration in the drift tube. In this framework, the measurements are assumed to be normally distributed and the average peak area and its uncertainty are determined through:

$$\overline{I_{mz}} = \frac{\sum^N I_{mz}}{N}, \tag{S6}$$

$$\sigma^2_{I_{mz}} = \frac{\sum^N (I_{mz} - \overline{I_{mz}})^2}{N}. \tag{S7}$$

Note that this assumption increases uncertainty when abrupt changes of ambient signal (e.g., due to local pollution) occurred. The precision inferred from the distribution during these periods is expected to be higher than that from the accumulated counts.

The combined precision on mixing ratios take into account the statistical uncertainties related to (i) count rate, (ii) background measurements, (iii) the normalization factor, and, for calibrated compounds, (iv) the calculated sensitivity obtained during the calibrations. It is calculated as follows:

$$\sigma^2_{\text{VMR}} = \left(\frac{\sqrt{\sigma^2_{I^*_{mz}(\text{ambient})} + \sigma^2_{I^*_{mz}(\text{background})}}}{I^*_{mz}(\text{ambient}) - I^*_{mz}(\text{background})} \right)^2 + \left(\frac{\sigma_{S_{X,mz}}}{S_{X,mz}} \right)^2, \tag{S8}$$

with:

$$\sigma^2_{I^*_{mz}} = \left(\frac{\sigma_{I_{mz}}}{I_{mz}} \right)^2 + \left(\frac{\sqrt{(488 \cdot \sigma_{I_{21.022}})^2 + (669 \cdot X_r \cdot Tr^{-1}_{38.033} \cdot \sigma_{I_{38.033}})^2}}{488 \cdot I_{21.022} + 669 \cdot X_r \cdot Tr^{-1}_{38.033} \cdot I_{38.033}} \right)^2. \tag{S9}$$

To calculate the systematic uncertainty (accuracy) on volume mixing ratios of signals related to compounds included in the calibration mixture, we combine the stated uncertainty of the concentrations in the bottle (Tab S2) with the uncertainty of the dilution system. The systematic uncertainty of mixing ratios quantified using the kinetic approach were set to 56%, which is obtained by combining an estimated accuracy of 25% on the value of k and 50% on the value of $FY_{X,mz}$ (in Eq. S3). This accuracy is close to results by Sekimoto et al. (2017) which showed that measured sensitivities agreed within 20–50% with theoretical sensitivities calculated using molecular mass, elemental composition, and functional group of the analyte.

A combined expanded uncertainty is calculated through:

$$\text{expanded uncertainty} = 2 \cdot \sqrt{\text{precision}^2 + \text{accuracy}^2} \tag{S10}$$

For the combined uncertainty, Simon et al. (2023) included an additional 5% uncertainty due to relative humidity effects. As the $H_3O^+(H_2O)$ signal was generally less than 3% that of $H_3O^+ + H_3O^+(H_2O)$

(Fig. S4), the impact of relative humidity was estimated to be small and no additional uncertainty is considered here. However, an additional uncertainty of 100% was taken into account for the expanded uncertainty of formaldehyde due to back-reaction in the drift tube owing to similar proton-affinities of HCHO and H_2O.

The limit of detection (quantification) was defined as three (ten) times the precision of the associated background measurement, of which we only considered the last 5 min to assure an equilibrium. The mean and standard deviation of the measurement distribution during these 5 min were used to define the background value and its precision, respectively.

S2.1.5 PAP configuration

The PTR-MS data was processed in segments of 24 hours. To combine outputs from different IDA analyses, m/z peak areas were associated to the DBSCAN cluster averages and concatenated. If more than one peak was present in the cluster, the sum of both was used for the total peak area associated to the cluster. The transmission and calibration factors were retrieved from the nearest valid calibration. When valves were switched in the manifold to sample from a different line or perform zero/calibration measurements, 5 seconds before the change and 30 seconds after were invalidated to allow for the flows to settle back to an equilibrium. A zero/calibration measurement must last at least 25/70 minutes in order to be considered. Calibrations were processed by considering 20 second accumulated peak areas to reduce uncertainty on calculated transmissions and sensitivities. Backgrounds related to a measurements must occur within the PAP 24-hour processing interval considered by the PAP. The background signal was interpolated for measurements in between two zero intervals. At the end/start of the PAP 24-hour processing interval, the nearest background measurement was used. When no zero measurement was present in the period, no data was processed. For masses related to compounds not included in the calibration standard, the PAP provides initial concentration estimates based on a standard collision rate of $2 \cdot 10^{-9}$ cm^3 molecule^{-1} s^{-1} without considering fragmentation or proton transfer yields. There is an option to refine collision rate constants, isotopic factors, and proton-transfer/fragmentation yield values in the PAP which was provided for preliminary analysis.

S2.2 PAP post-processing

S2.2.1 Updated sensitivity

The PAP processing routines provided concentrations for all m/z clusters identified with DBSCAN and included in the final list of retained masses. While concentrations related to calibrated signals were final in the PAP output, those associated with other masses were based on a rudimentary estimates of their sensitivity. As such, their concentrations were only suitable for preliminary analysis. Evolving insights in tentative compound identification, and associated changes in sensitivities, required transformation of preliminary concentration estimates to the most up to date information available. As a result, a PAP post-processing was run to adjust the concentrations to the latest sensitivity information (Table S3).

S2.2.2 Concentration flagging

Aside from the invalid flag around switching valves in the sampling manifold (Sect. S2.1.5), minimal flagging of data was applied for generating data at 10 Hz frequency. For the 1 min concentrations, additional flags were introduced related to either data quality and occurrences of plumes originating from the nearby saw-mill.

Several instances related to data quality have been identified. First, to account for the instrument response time when introducing high gradients in concentrations, we considered how concentrations evolved during zero measurement intervals. We calculated how fast concentrations were consistent with a zero measurement (i.e., limit of detection within the measurement precision) from an exponential fit to the median uncertainty weighed distance for the limit of detection after starting a zero measurement (Fig. S1). In general, three behavioural patterns were identified: (i) considerable recovery time ($t_d > 1$ min), (ii) negligible recovery time ($t_d < 1$ min), and (iii) exponential fit invalid. Only in the case of considerable recovery time, additional data were flagged as invalid after zero measurements. Occurrences of the invalid exponential fit show a good correspondence with zero immediately after zero-air is being sampled and thus no invalid measurements have been considered after returning to ambient measurements.

Second, a manual flagging was applied to periods where there were some technical challenges affecting the data quality. Data associated to these periods have been flagged as invalid and were not reported in the 1 min VOC database. A last flag associated with data quality is related to the significance of the data and indicates when a measurement is below the theoretical limit of detection.
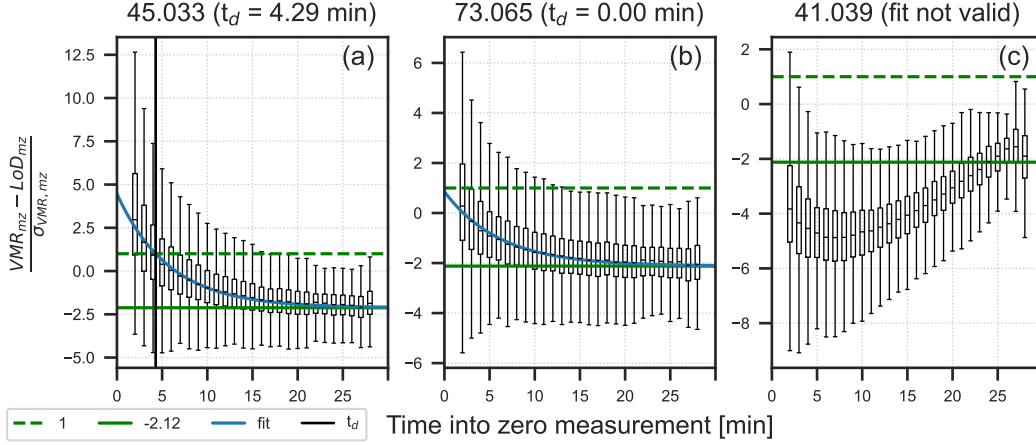
Figure S1: Evolution of distribution of differences between volume mixing ratio and the limit of detection divided by the measurement precision after switching from an ambient measurement to a zero measurement for signals at m/z 45.033 **(a)**, 73.065 **(b)**, and 41.039 **(c)**. The first and last measurements are flagged as invalid (Sect. S2.1.5) and not taken into account for this analysis. At a value of 1 (dashed green line), the measurement is consistent with zero. At a volume mixing ratio of zero, this value is expected to be at $\sim$ -2.12 (solid green line). An exponential function is fit to the median time evolution (blue curve) and we estimate the recovery time (t_d, vertical solid black line) as the time where the fit intersects with 1.

Local sources affecting our data were limited to the impact of plumes originating from the local wood factory. The flags recorded in the 1 min VOC database were obtained by applying the *flag_plume* determined for filtering EC fluxes. Any interval of 30 minutes for which no flux was determined (e.g., measurements in the PROFILE configuration, incomplete half hour data, or periods where no 3D wind data was available at the sampling location) were not flagged because of this.

S2.3 PTR-ToF-MS instrument performance

S2.3.1 Calibrations

The variation of calculated sensitivities and transmissions during the different campaigns is shown in Fig. S3. The resulting transmission curves are shown in Fig. S2. Calibration stability was quantified for all compounds included in the calibration standard by the relative standard deviation of the peak area during the last hour of the calibration interval. When the calibration stability was two standard deviations away from the mean of the calibration stability distribution from the whole campaign, it was flagged as unstable. If more than four masses were flagged as unstable during the same calibration, we consider the calibration as a whole to be unstable. As a result, we did not consider the calculated sensitivities and transmissions. Periods for which the nearest calibration was considered unstable are estimated to possibly be subject to instrument instabilities. As a result, no concentrations were calculated for these periods.

S2.3.2 Ion source impurities

Figure S4 shows the distribution of primary source ions relative to the normalization factor. For quality assurance, the ACTRIS standards for operation (Dusanter S. et al., 2025) suggest using a 3% and 20% threshold for $O_2^+ + NO^+$ and $H_3O^+(H_2O)$ impurities, respectively. Because the PTR-ToF-MS was operated at a E/N value of 135 Td, the influence of the water cluster is expected to be limited. Indeed, as we can see, the watercluster typically contributed to only $< 3\%$ of the $H_3O^+ + H_3O^+(H_2O)$ signal. While the other impurities were conforming to the 3% limit during the 2023 campaign, the 2022 and 2024 campaigns had periods where this threshold was crossed. An alternative method to quantify the O_2^+ impurity is by considering the ratio between the signal (cps) observed at m/z 78.046 and 79.054. The signal at the lowest mass is originating from $C_6H_6 + O_2^+$ while the signal at the highest mass is originating from $C_6H_6 + H_3O^+$. As benzene is about equally sensitive to reaction with both primary ions, their ratio provides a good estimate on the impact of O_2^+ in the spectrum. As we see from Fig. S4, the influence of O_2^+ varied from $1 - 6\%$ over the three campaigns. When considering both impurities, we concluded that the quality of our setup was sufficient.
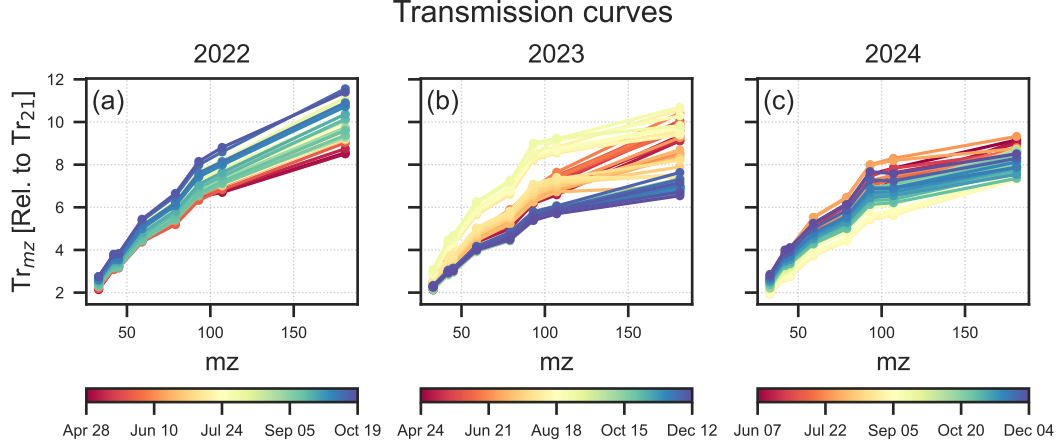
Figure S2: Transmissions curves as determined during calibrations in 2022 **(a)**, 2023 **(b)**, and 2024 **(c)**. The transmission is defined relative to the transmission at m/z 21.022 (i.e., $Tr_{21.022} \equiv 1$) and transmissions above m/z 180.937 are considered to be constant (i.e., $Tr_{mz>180.937} \equiv Tr_{180.937}$).
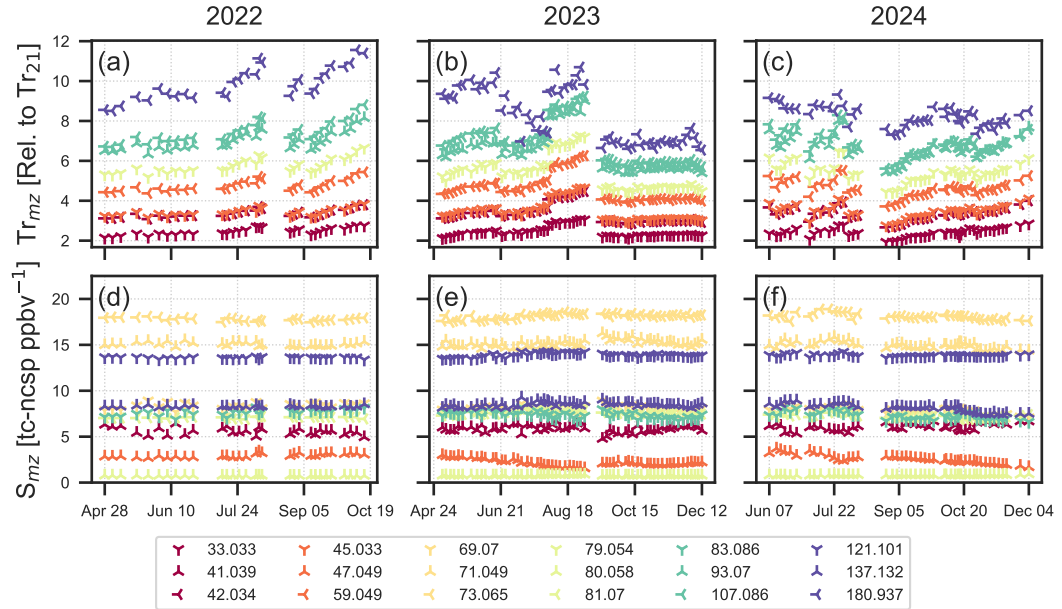

Figure S3: Evolution of transmission **(a–c)** and sensitivity **(d–f)** obtained during validated calibrations during the 2022 **(a,d)**, 2023 **(b,e)**, and 2024 **(c,f)** campaigns.
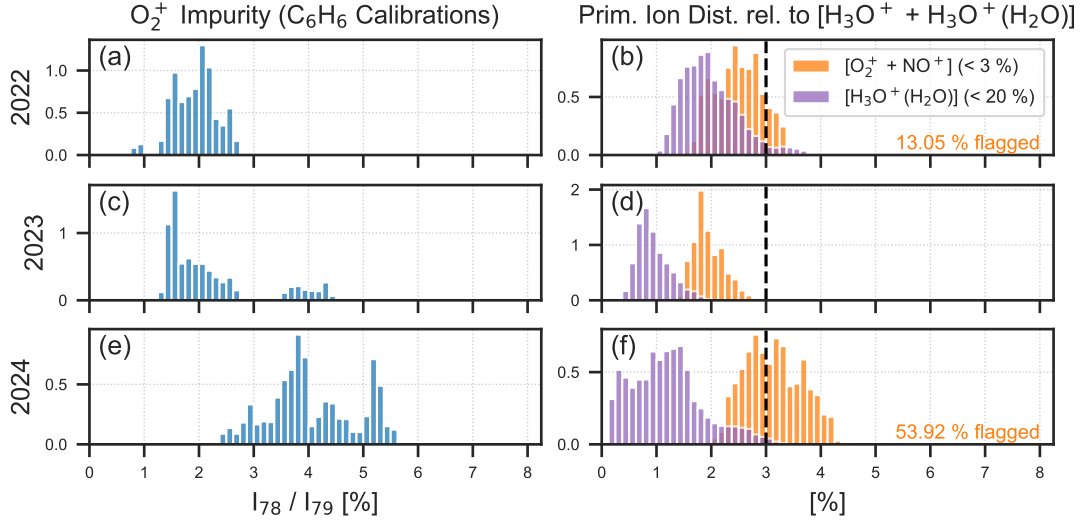
Figure S4: Data quality and assurance for primary ion signal purity. On the left side we see the distribution the signal related to benzene observed at m/z 78 (from reaction with O_2^+ impurity ions) relative to its signal at m/z 79 (from reaction with H_3O^+) for 2022 (a), 2023 (c), and 2024 (e). This ratio is only calculated during calibrations when the signal related to benzene at m/z 79 is not affected by the cluster from hydrated acetic acid. On the right we show the signal from $NO^+ + O_2^+$ (orange) and $H_3O^+(H_2O)$ (purple) relative to $H_3O^+ + H_3O^+(H_2O)$ for 2022 (b), 2023 (d), and 2024 (f).

S3 Fluxes

S3.1 Filtering of low turbulence conditions

Theoretically, turbulent fluxes measured by the EC technique should be discarded below a given friction velocity (u^*) threshold to avoid night-time flux underestimation errors (Aubinet et al., 2012). This so-called night flux error was first demonstrated for CO_2 fluxes: below a certain u^* value, nighttime CO_2 fluxes tend to decrease, despite the fact that their main drivers—plant and soil respiration—are expected to be independent of turbulence. This discrepancy is generally explained by the increasing importance of advection under low-turbulence conditions. When only the turbulent component is considered, this leads to an underestimation of the net exchange (Aubinet et al., 2012). For this reason, applying a u^* threshold is standard practice for CO_2 fluxes.

However, when the production/deposition mechanism is directly influenced by turbulence, the application of a u^* filter is not recommended (Aubinet et al., 2012). Fig. S5 shows the relationship between night-time fluxes and u^* for three trace gases. Since u^* is often correlated with other environmental variables, especially air temperature, this could confuse the interpretation. To minimize this effect, monoterpene (m/z 137.132) and methanol (m/z 33.033) fluxes were normalized using the light-independent response function proposed by Guenther et al. (2012). Ozone fluxes were not normalized.

In all three cases, absolute nighttime fluxes decrease at low u^*, but this trend may reflect real processes rather than measurement artefacts. For methanol and ozone (panels b and c), which exhibit night-time uptake, the fluxes are thought to result from diffusive exchange between the atmosphere and a reservoir. Such deposition processes are partly governed by a resistance to diffusion, which depends on turbulence (and thus on u^*). Furthermore, low turbulence can increase the atmospheric residence time, potentially affecting chemical reactions and loss rates. For gases with such dynamics, filtering based on u^* may exclude meaningful fluxes and is therefore not appropriate. Similar conclusions were reached by Bachy et al. (2018)

In contrast, monoterpene fluxes (panel a) show a pattern more similar to that observed for CO_2, with relatively stable normalized fluxes at high u^* and a sharp decline below 0.45 m s^{-1}. This threshold is close to the value found for CO_2 at the same site (0.4 m s^{-1}, Aubinet et al. 2018). However, unlike CO_2, there is no strong evidence that monoterpene emissions are independent of turbulence. The observed decline may thus reflect a true dependency of emission on u^*. To avoid excluding important periods from the analysis, no u^* filtering was applied to monoterpenes or any other trace gas measured in the present study.
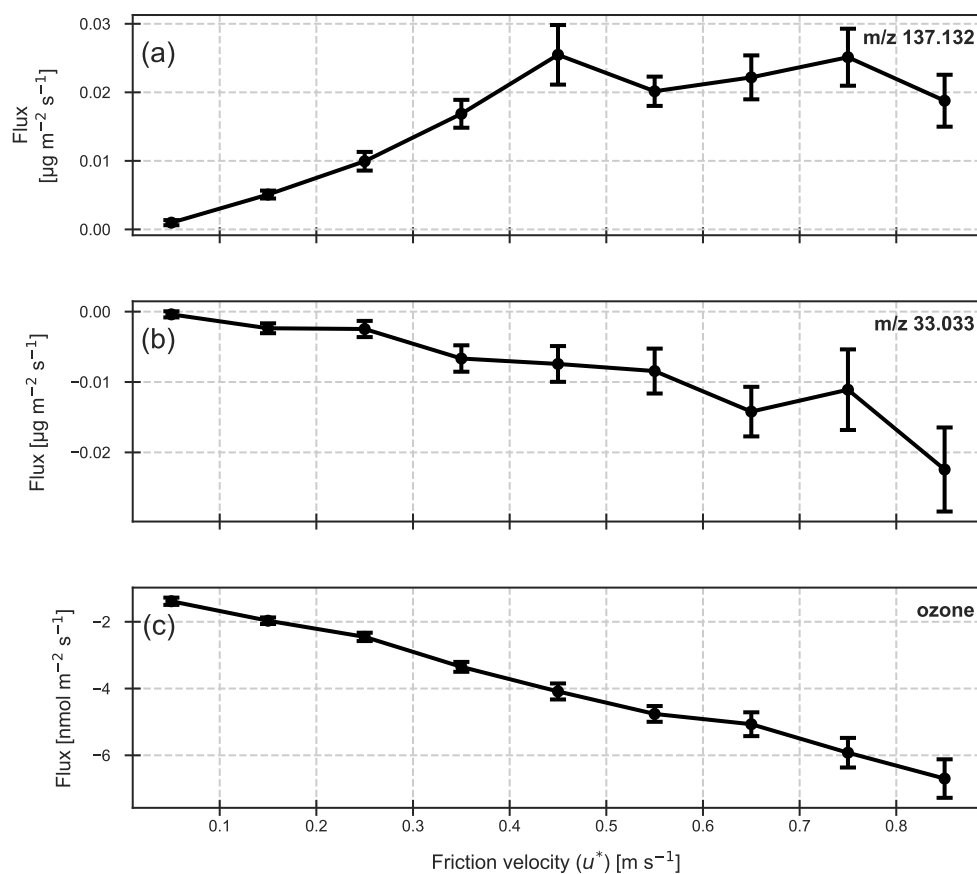
Figure S5: Relationship between night-time fluxes and friction velocity (u^*). Mean fluxes (circles) are shown per binned u^* class, with bars indicating standard deviations. **(a)** Normalized fluxes of m/z 137.132 (sum of monoterpenes). **(b)** Normalized fluxes of m/z 33.033 (methanol). **(c)** Non-normalized ozone fluxes.

S3.2 Planar fit vs. double rotation

As detailed in . 2.3.3 of the main document, the double rotation method resulted in a higher number of outliers in TRUNK fluxes compared to the sector-wise planar fit method (Fig. S6). This effect is illustrated here for ozone fluxes during the year 2023, but was also consistently observed for all VOCs and across all years.

No such effect was observed for TOP fluxes, for which the double rotation method was therefore retained.
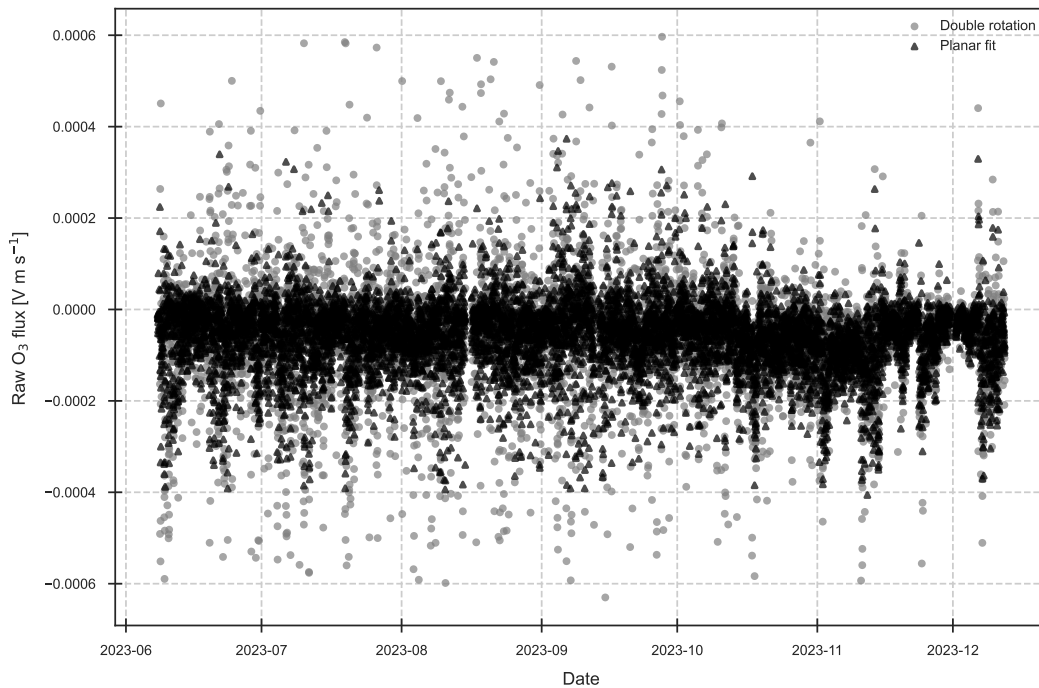

Figure S6: Comparison of raw ozone fluxes computed for year 2023, TRUNK system, with the double rotation method vs. planar fit method.

S3.3 Correction for flux high-frequency losses

The transfer function of monoterpene fluxes measured at the TOP system was well defined, with a half-power cut-off frequency of 0.11 Hz (Fig.S7). The associated correction factors ranged from 1.10 to 1.23 under unstable conditions, and from 1.23 to 1.26 under stable conditions (Fig.S8). Although the cut-off frequency was low due to the characteristics of the air sampling system, the resulting correction factors remained reasonable because the high-frequency signal content was limited by the large measurement height. The choice to use the square root of the Lorentzian transfer function, as suggested by Peltola et al. (2021), although theoretically sound, had little effect on the fit quality (Fig. S7) and only a limited impact on the correction factor (ranging between 1.1 and 2.5%, depending on wind speed and stability). Applying the same approach to isoprene yielded similar results, whereas other compounds did not allow for a robust estimation of the cut-off frequency (not shown).

For the TRUNK system, correction factors for monoterpene fluxes under unstable conditions fell within the lower range of those observed for the TOP system, due to lower wind speeds (Fig. S8). However, under stable conditions, they were equal to or even higher than those of the TOP system, as the high-frequency content of the covariance was greater in the trunk space in these conditions (not shown).

In contrast to VOCs, the determination of the cut-off frequency for ozone was possible not only for the TOP but also for the TRUNK system, due to more pronounced TRUNK fluxes. The half-power cut-off frequencies were 0.11 Hz for the TOP and 0.33 Hz for the TRUNK system (Fig.S9). This difference can be attributed to the longer sampling tube of the TOP system (6.5 m) compared to the TRUNK system (5 m), with other setup characteristics being similar. The associated correction factors were always below 1.4 and were lower for the TRUNK than for the TOP system, and also lower than those calculated for TRUNK monoterpene fluxes, mainly due to the higher cut-off frequency (Fig.S10).
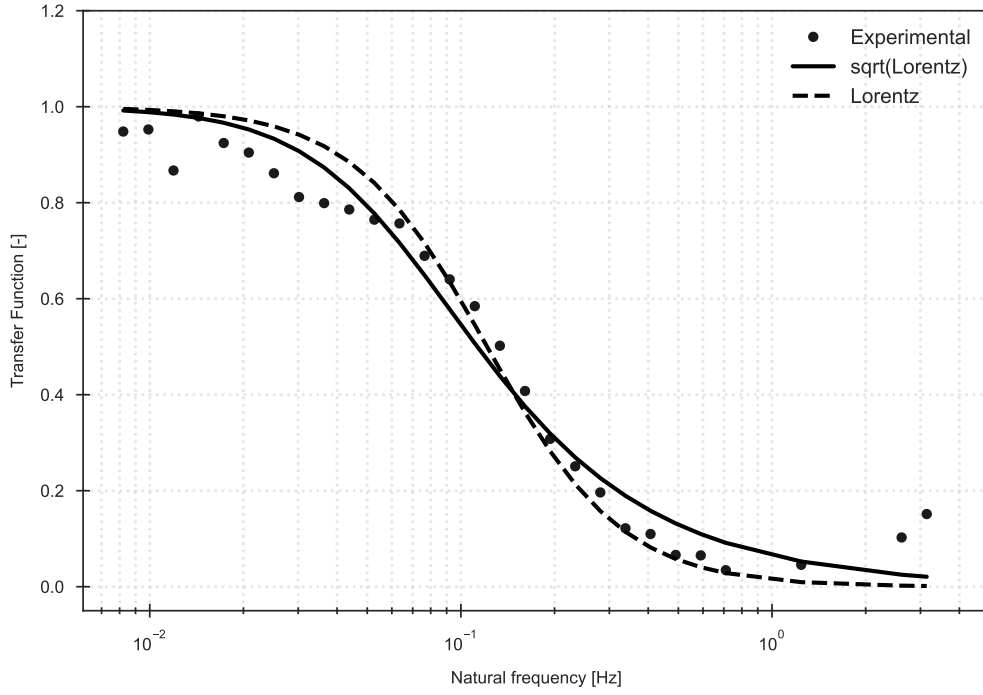
Figure S7: Experimental transfer function of monoterpene fluxes for the TOP system (points). The fits are performed with the square root of the Lorentzian transfer function and the Lorentzian transfer function, respectively (see main text). 2023 data were used and filtered for high (> 50 W m^{-2}) and quality-filtered sensible heat fluxes and high (> 0.142 μg m^{-2} s^{-1}, 90$^{\text{th}}$ percentile) and plume-filtered monoterpenes fluxes, ending in 312 half-hours.
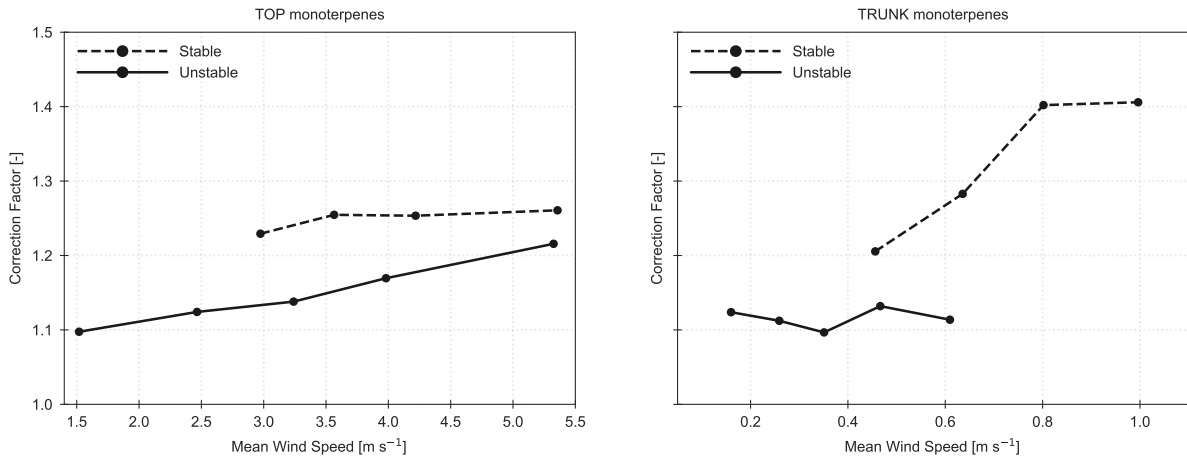

Figure S8: Dependence of the monoterpene co-spectral correction factor on horizontal wind speed, for TOP and TRUNK systems, and for unstable and stable conditions.
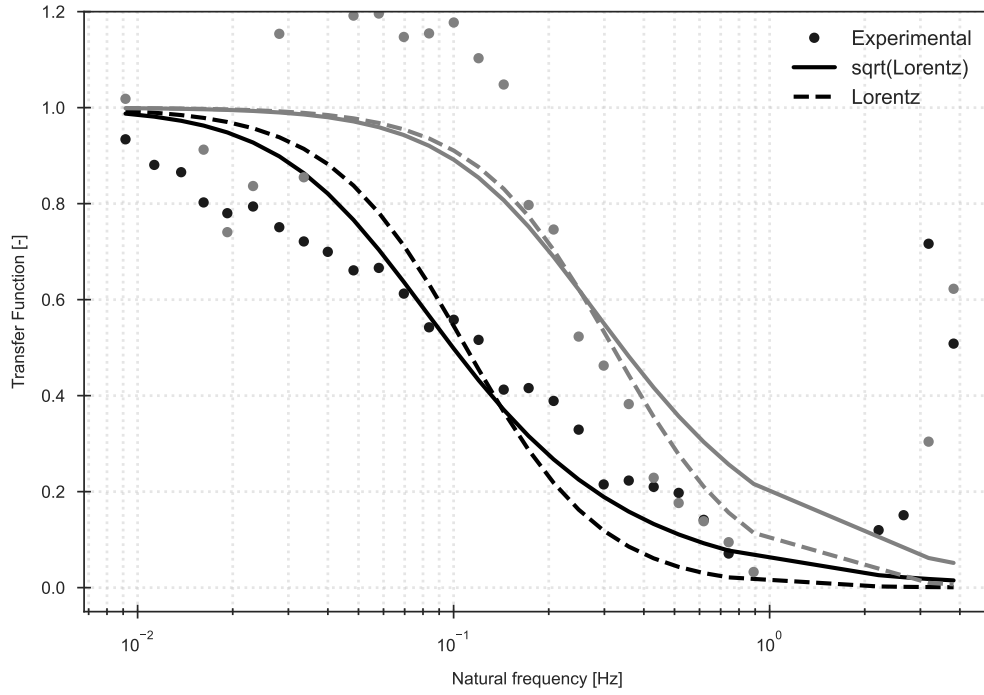
Figure S9: same as Fig. S7, but for ozone TOP (black) and TRUNK (grey) systems. Data filtering was the one described in Sect. 2.4.1, ending in 225 and 965 half-hours for TOP and TRUNK, respectively.
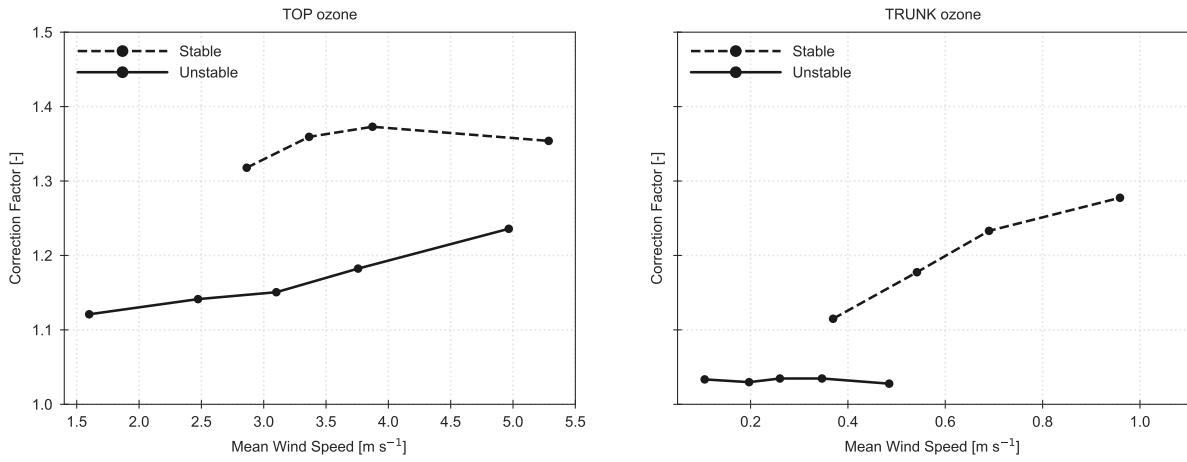

Figure S10: same as Fig. S8, but for ozone.

S3.4 Flux flagging

As illustrated in Fig. S12, compounds that were most frequently flagged were monoterpenes (m/z 137.132) and their fragment (m/z 81.070), as well as methanol (m/z 33.033). These VOCs were predominantly affected by plumes originating from the wood factory located 3 km south-west of the flux tower. Among the three flags, *flag_MF* was the one most frequently raised. This flag comprises a stationarity or steady-state test (SST) and an integral turbulence characteristic (ITC) test. The ITC assumption was generally validated, so that *flag_MF* is mainly linked to the SST. Many nighttime periods were found to be non-stationary, which is a common occurrence in EC measurements, but the SST also successfully identified numerous half-hour intervals affected by plumes, though not all. The *flag_plume*, specifically designed to filter out such events, performed well at detecting affected VOCs (Fig. S11), and in most cases, was strongly correlated with *flag_MF*. Many half-hours were flagged by both *flag_MF* and *flag_plume*, so the percentage for *flag_tot* does not correspond to the arithmetic sum of the three individual tests.

At the TRUNK level, plume events identified by *flag_plume* were observed less frequently. This is expected as such plumes were likely transported at higher altitudes, more directly affecting the concentrations measured at the TOP level. In contrast, *flag_MF* was triggered more often at the TRUNK level. As with the TOP system, this was mainly due to SST. This may reflect the fact that this test was originally designed for above-canopy fluxes and may not be well suited to below-canopy turbulent fluxes. To our knowledge, no comprehensive and standardized methodology for filtering below-canopy flux measurements has been established, despite the first such measurements dating back to the 1980s. Given the small magnitude of our TRUNK fluxes, we did not attempt to develop a specific flagging procedure for this level and instead applied the same criteria as used for the TOP fluxes.
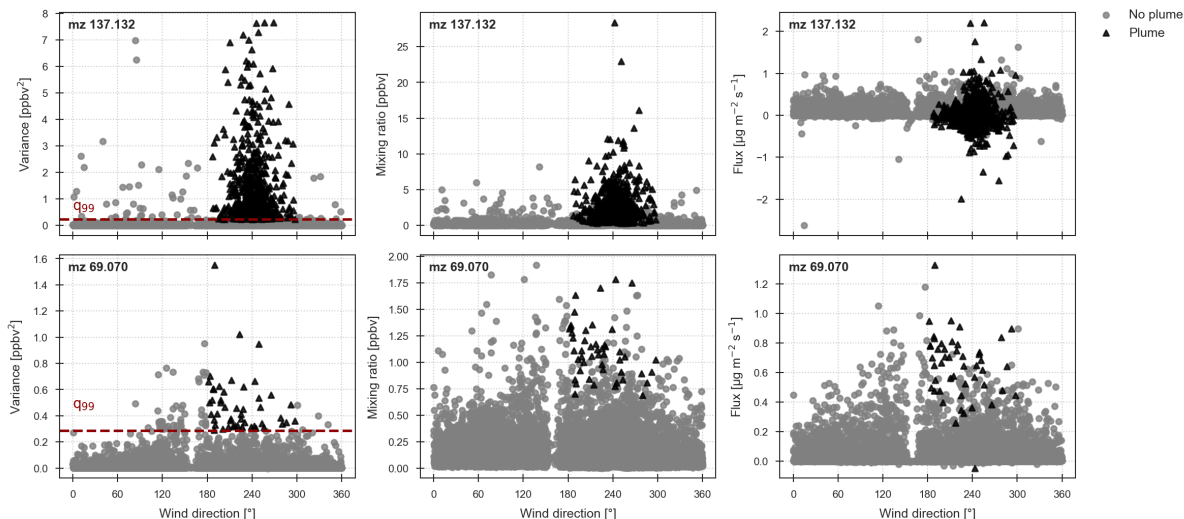

Figure S11: Effect of plume events on concentration variance, mean concentration and fluxes of m/z 137.132 (protonated monoterpenes) and m/z 69.070 (protonated isoprene) for all years, TOP system. The flagging is based on q_{99}, the 99th percentile of the concentration variance calculated across all wind directions, except 180-300°.

S3.5 Ozone flux calibration

Fig. S13 shows how the percentage of calibrated half-hours (where $R^2 > 0.5$) increases with data accumulation, while the calibrated flux error initially decreases before stabilizing or even increasing. The initial improvement in fit quality (R^2) results from the attenuation of random fluctuations (instrumental white noise), as longer periods provide more data points. However, this benefit is gradually offset by changes in the sensitivity of the FOS, which degrade the correlation between the FOS and the T400. Consequently, R^2 plateaus, and for periods exceeding 24 hours (up to a disc lifetime, data not shown), the proportion of calibrated data decreases.

The evolution of the calibrated flux error follows similar principles: initially decreasing due to white noise reduction, then increasing/stabilizing as the relationship shifts. However, the optimal period for minimizing flux error does not coincide with the one maximizing R^2. For example, with the TRUNK system in 2023 (panel d), the median calibrated flux error rises sharply for periods longer than 2 hours, although the proportion of calibrated half-hours continues to grow.
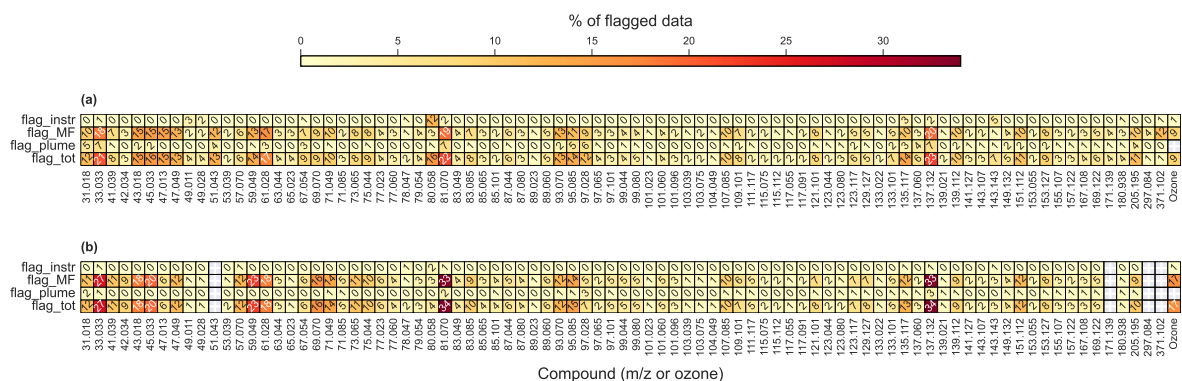
Figure S12: Percentage of flux data flagged by the different quality flags, for each m/z value and for ozone. *flag_instr* for instrumental problems; *flag_MF* for flag according to Mauder & Foken policy; *flag_plume* for filtering anthropogenic sources (wood factory); *flag_tot* for the combination of the three flags above.
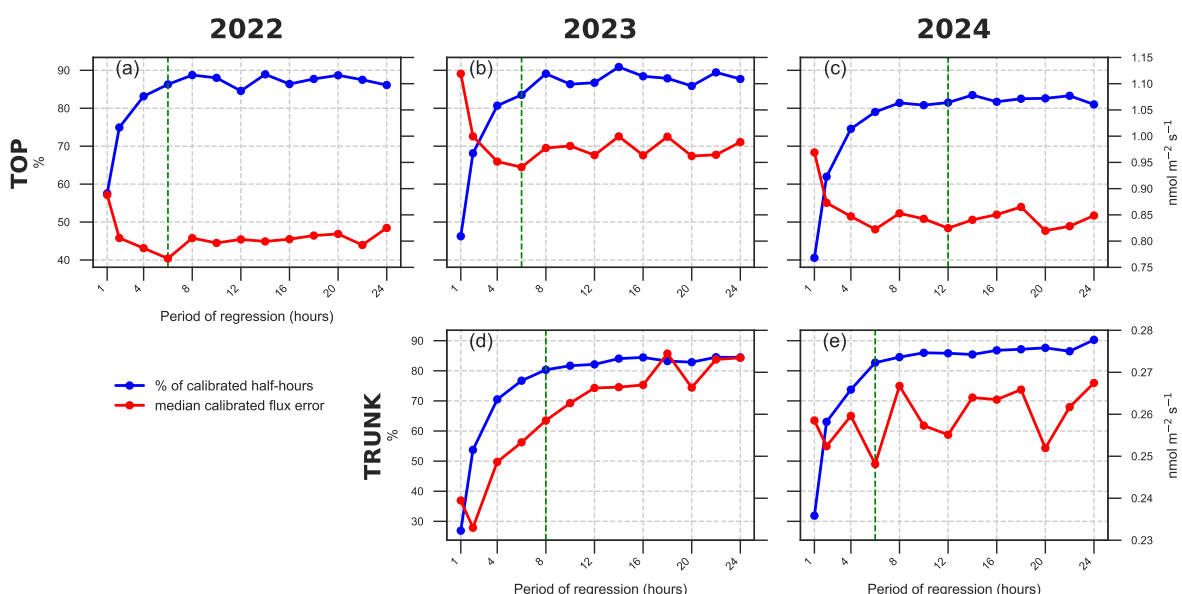

Figure S13: Evolution of the percentage of calibrated half-hours and the median calibrated flux error, as a function of the period used for T400 vs. FOS regressions for years 2022, 2023 and 2024, and TOP vs. TRUNK systems. The green dashed line indicates the regression period for which the optimum between maximum percentage and minimum error was found.

Differences between panels can be attributed in part to the varying coverage of the data. While FOS analysers operated continuously, T400 measurements were divided between systems. For example, in 2022, about 70% of the half-hours were dedicated to the TOP system, whereas in 2023 and 2024, the addition of the TRUNK system resulted in the availability of combined FOS and T400 data for approximately 50% and 20% of the half-hours, respectively. The amount of data available for a given regression period partly explains the discrepancies between TOP and TRUNK panels.

For each year and system, an optimal regression period was chosen. For the TOP system (panels a, b, c), the selection was straightforward—minimizing the calibrated flux error and coinciding with the onset of R^2 stabilization. For the TRUNK system, particularly in 2023 (panel d), the choice was more subjective. Here, we prioritized a higher proportion of calibrated half-hours, despite a higher flux error. It is worth noting that in 2024, despite much less frequent disc replacements for the TOP system (up to 36 days compared to a week in 2022 and 2023), the proportion of calibrated data and the flux error were not significantly affected, highlighting the potential to reduce workload without compromising data quality.

S3.6 Ozone storage

Ozone storage was negative at night (Fig. S14), indicating a depletion below the EC measurement level. The storage flux became positive on average around 06:00 LT for both the TOP and TRUNK levels. This timing corresponds to the transition from stable night-time to turbulent daytime conditions, as well as to the onset of photochemical processes favouring O_3 production. Air enriched in ozone is transported into the canopy, ozone uptake increases sharply, and part of the ozone accumulates within the canopy air space. Storage fluxes peaked around 09:00–10:00 LT, then gradually decreased, becoming negative again around 15:00–16:00 LT. The most negative storage flux values were observed in the late evening, around 20:00 LT.

Neglecting O_3 storage would lead to an underestimation of evening and night-time deposition, and an overestimation of daytime uptake. Daytime ozone accumulation can lead to a maximum mean storage of approximately +1.5 and +0.18 nmol m^{-2} s^{-1} for the TOP and TRUNK systems, respectively representing a correction of about 17% of the turbulent flux. The strongest negative storage values reached around –1 and –0.1 nmol m^{-2} s^{-1}, corresponding to corrections ranging from 24 to 59%. For comparison, the magnitudes observed here are approximately four times lower than those reported by Finco et al. (2018) in a mixed oak–hornbeam forest in northern Italy. Despite the lower magnitudes, the corrections were applied, considering their potential impact on the flux estimates.
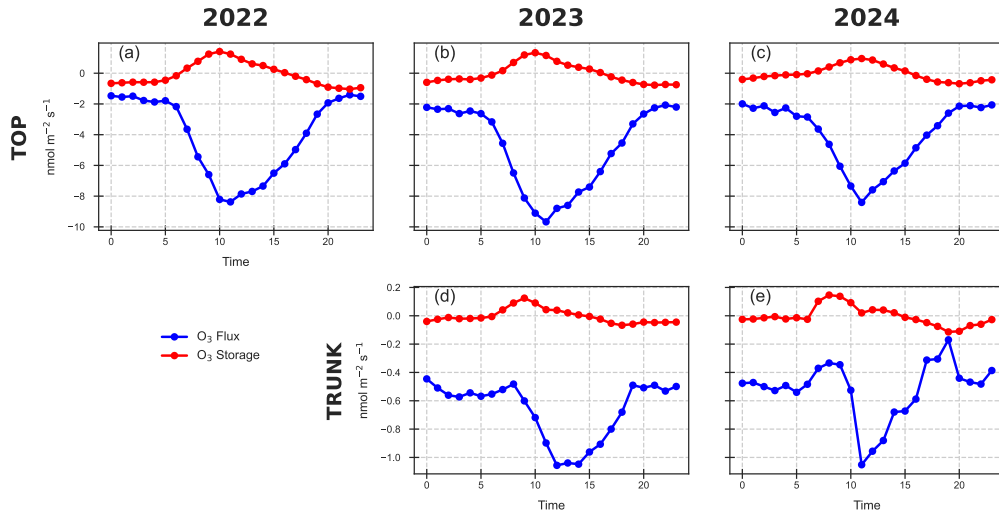

Figure S14: Diel evolutions of ozone calibrated flux and ozone storage for the TOP (a-c) and TRUNK (d-e) systems, over years 2022, 2023 and 2024.
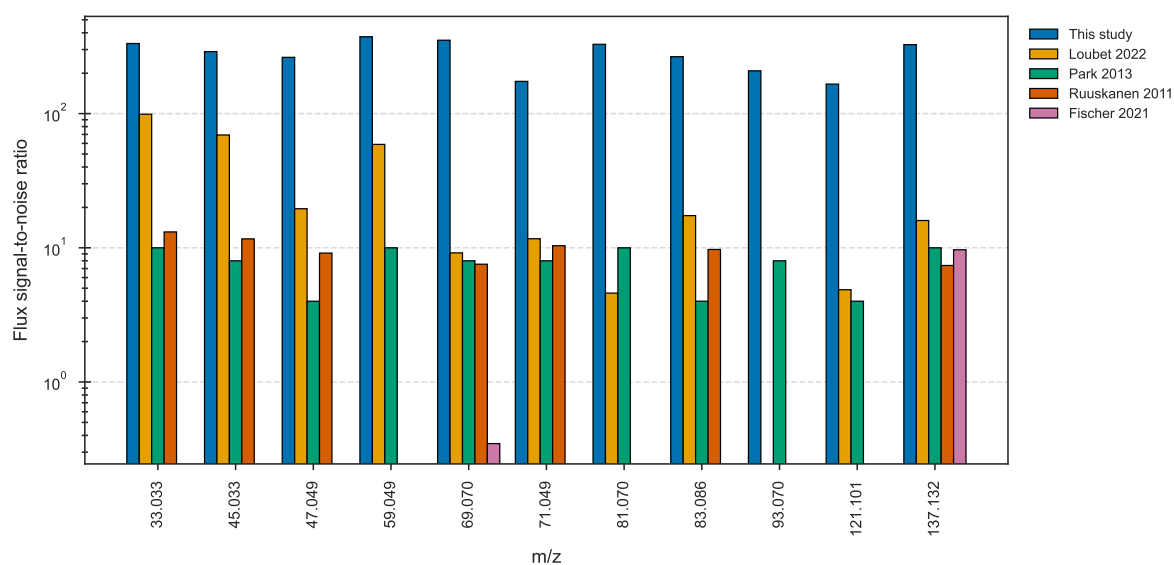
S3.7 VOC flux signal-to-noise ratio

Figure S15: Comparison of flux signal-to-noise ratio across studies for a subset of VOCs. The flux signal-to-noise ratio is defined as the mean flux divided by the average flux random noise and is represented in log scale.

S3.8 VOC flux balance
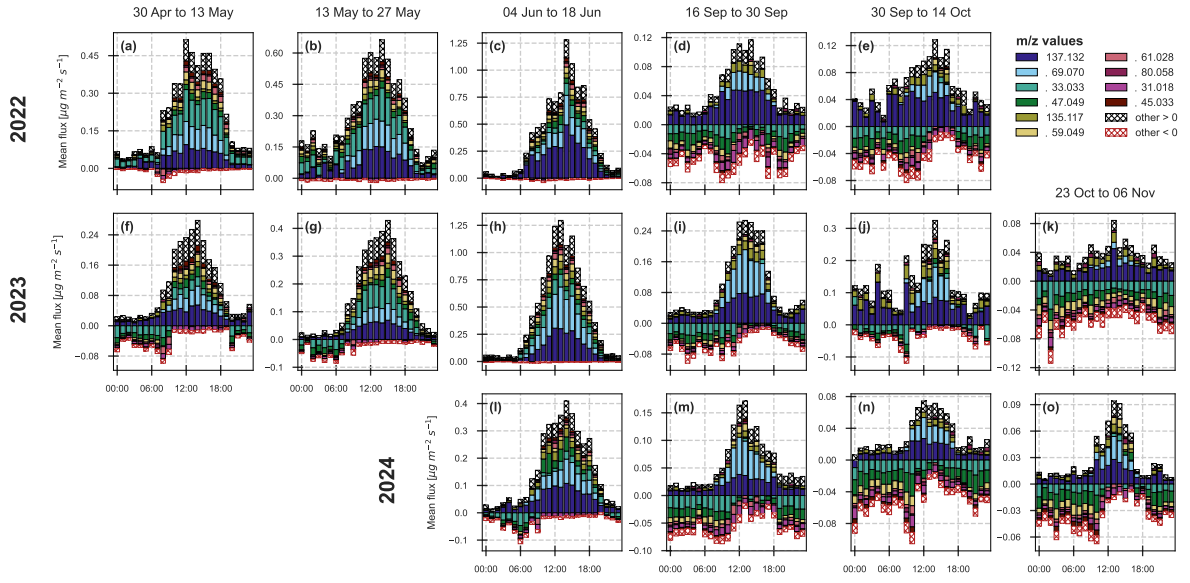
Figure S16: Seasonal evolution of VOC fluxes measured by the TOP system over the years 2022 (a-e), 2023 (f-k), and 2024 (l-o). For each m/z value and hour of the day (in LT), mean fluxes are calculated only when at least 25% of the expected half-hourly data are available within the corresponding period. The 10 most exchanged m/z values are shown individually (see legend), while the remaining compounds are grouped into emission ("other > 0") and deposition ("other < 0") categories. Compared to Fig. 8 presented in the main text, all panels have distinct y-axis limits.

S4 List of detected VOC-related ions

Table S3: List of exact m/z values and corresponding chemical formula associated to the 74 clusters selected for concentration quantification. Column description: tentative compound attribution (third column), polarizability (fourth column), dipole moment (fifth column), collision rate constant (sixth column), proton transfer (PT) yield or fragment yield (seventh column), reduced electric field (detailed below, eighth column), resulting calculated sensitivity for individual compounds (S_{ind}; ninth column), overall sensitivity used for deriving concentrations (S_{mz}; tenth column), and 3-year average limit of detection with the associated standard deviation from 1 min concentrations (LoD; eleventh column). For m/z values that are attributed to fragments of nascent excited protonated compounds, the integer molecular mass of the compound is mentioned between brackets. Where PT or fragment yields are available from specific studies, the reduced electric field (E/N) is mentioned in the eighth column where available (NA otherwise). Compounds included in the calibration standard are highlighted with grey backgrounds and their sensitivity (average over all three campaigns) is reported (boldface S_{mz} values). Compounds observed in biogenic environments (Kim et al., 2010; Hellén et al., 2018; Schallhart et al., 2018; Pfannerstill et al., 2021) are highlighted in brown and bold.

m/z	Chemical Formula	Tentative Compound Attribution	Polarizability (10^{-30} m^3)	Dipole moment (Debye)	k_{coll} (10^{-9} cm^3 molec^{-1} s^{-1})	PT or fragment yield (%)	E/N (Td)	S_{ind} (tc-ncps ppbv^{-1})	S_{mz} (tc-ncps ppbv^{-1})	LoD (pptv)
31.018	CH$_2$OH$^+$	**formaldehyde** frag. methylhydroperoxide, ethanol, . . .							5.10[*]	29 (11)
33.033	CH$_4$OH$^+$	**methanol**							**13.63**	21 (10)
41.039	C$_3$H$_4$H$^+$	**frag. isoprene (68 u)**							**5.92**	14 (5)
		1,2-propadiene	6.11[b]	0.00[b]	1.61	100[std]		9.84		
		propyne	6.18[a]	0.78[a]	1.73	100[1]	106	10.55		
		cyclopropene	5.18[b]	0.48[b]	1.52	100[std]		9.29		

m/z	Chemical Formula	Tentative Compound Attribution	Polarizability (10^{-30} m^3)	Dipole moment (Debye)	k_{coll} (10^{-9} cm^3 molec^{-1} s^{-1})	PT or fragment yield (%)	E/N (Td)	S_{ind} (tc-ncps ppbv^{-1})	S_{mz} (tc-ncps ppbv^{-1})	LoD (pptv)
		frag. acetone, 2-methylbutyric acid, 1-octen3-ol, 2-ethyl-1-hexanol, 3-methyl-1-butanol,2-methyl-3-buten-2-ol, 3-methyl-2-buten-1-ol, 3-methyl-3-buten-1-ol, ethyl butanoate, ethyl-2-methyl propanoate, hexanol, hexyl acetate, methacrolein methacrylic acid, nonanal, propane-1,2-diol, pentanal, propanal								
42.034	C$_2$H$_3$NH$^+$	**acetonitrile** isocyanomethane							**23.2**	2.0 (0.9)
43.018	C$_2$H$_2$OH$^+$	**frag. acetic acid (60 u)** ketene fragments of 2,3-butanedione, acrylic acid, methyl vinyl ketone, isopropanol, n-propanol, hexyl acetate, methyl acetate	5.10[a] 4.29[b]	1.70[a] 1.52[b]	2.07 2	51 (5)[2] 100[std]	135	6.62 12.3	6.62[z]	16 (7)
45.033	C$_2$H$_4$OH$^+$	**acetaldehyde** ethylene oxide							**18.19**	4.3 (1.7)
47.013	CH$_2$O$_2$H$^+$	**formic acid**	3.40[a]	1.43[a]	1.81	100[3]	130	11.37	11.37	13 (5)
47.049	C$_2$H$_6$OH$^+$	**ethanol** dimethyl ether							**2.5**	18 (7)
49.011	CH$_4$SH$^+$	methanethiol	5.62[c]	1.52[a]	2.02	100[std]		11.9	11.90[z]	2.5 (1.4)
49.028	CH$_4$O$_2$H$^+$	methanediol							7.85[u]	4 (2)
53.039	C$_4$H$_4$H$^+$	1-buten-3-yne	6.80[c]	0.22[a]	1.63	100[std]		9.74	7.85[u]	4 (3)

m/z	Chemical Formula	Tentative Compound Attribution	Polarizability (10^{-30} m^3)	Dipole moment (Debye)	k_{coll} (10^{-9} cm^3 molec^{-1} s^{-1})	PT or fragment yield (%)	E/N (Td)	S_{ind} (tc-ncps ppbv^{-1})	S_{mz} (tc-ncps ppbv^{-1})	LoD (pptv)
		cyclobutadiene								
57.070	C$_4$H$_8$H$^+$	**1-butene**	8.25[a]	0.35[b]	1.8	90[4]	120	9.77	7.85[x]	5 (2)
		cis-2-butene	7.64[a]	0.25[a]	1.72	89[4]	120	9.27		
		trans-2-butene	8.49[a]	0.00[5]	1.81	100[1]	106	10.95		
		frag. hexanol (102 u)	12.04[b]	1.60[a]	2.31	17[7]	NA	2.37		
						16[7]	NA	2.23		
		frag. cis-3-hexenyl acetate (142 u)	16.50[8]	2.00[8]	2.68	3[7]	NA	0.49		
		frag. hexyl acetate (144 u)	16.20[9]	1.86[9]	2.61	5[7]	NA	0.79		
		2-methylpropene	7.93[b]	0.57[b]	1.79	100[std]		10.8		
		frag. 1-butanal (72 u), frag. valeric acid	8.22[b]	2.71[b]	3	100[std]		18.14		
59.049	C$_3$H$_6$OH$^+$	**acetone**							**18.8**	5 (2)
		propanal	6.50[a]	2.72[a]	2.99	100[3]	130	18.09		
		2-propen-1-ol	6.82[b]	1.62[b]	2.11	100[std]		12.76		
		oxetane	6.02[b]	1.99[b]	2.38	100[std]		14.4		
		methyl vinyl ether, propylene oxide								
61.028	C$_2$H$_4$O$_2$H$^+$	**acetic acid**	5.10[a]	1.70[a]	2.07	49 (5)[2]	135	6.05	6.05[z]	11 (4)
						47-66[10]	132	5.93-8.32		
		glycolaldehyde	3.37[c]	2.73[a]	2.65	100[std]		16.16		
		methyl formate	5.05[a]	1.77[a]	2.13	100[std]		12.97		
		fragments of 2,3-butanedione, ethyl acetate								
65.023	CH$_4$O$_3$H$^+$	hydroperoxymethanol							7.85[u]	3.1 (1.6)
67.054	C$_5$H$_6$H$^+$	1,3-cyclopentadiene	8.64[a]	0.42[a]	1.81	100[std]		10.73	7.85[u]	2.7 (1.4)
		3-penten-1-yne								
		fragments of monoterpene and butanol								
69.070	C$_5$H$_8$H$^+$	**isoprene**							**8.03**	3.4 (1.3)

m/z	Chemical Formula	Tentative Compound Attribution	Polarizability $(10^{-30}$ m^3)	Dipole moment (Debye)	k_{coll} $(10^{-9}$ cm^3 molec^{-1} s^{-1})	PT or fragment yield (%)	E/N (Td)	S_{ind} (tc-ncps ppbv^{-1})	S_{mz} (tc-ncps ppbv^{-1})	LoD (pptv)
		trans-1,3-pentadiene	10.86[b]	0.72[b]	2.05	100[std]		12.16		
		cyclopentene	8.84[a]	0.20[a]	1.81	100[1]	106	10.73		
		2-pentyne	8.77[b]	0.66[b]	1.85	100[std]		10.95		
		cis-1,3-pentadiene								
		1,4-pentadiene,								
		3-methyl-1-butyne,								
		1-methyl-cyclobutene,								
		3,3-dimethyl-cyclopropene,								
		ethenylcyclopropane								
		fragments of myrcene,								
		levoglucosan,								
		2-methyl-3-buten-2-ol, prenol,								
		pentanal								
71.049	$C_4H_6OH^+$	**methyl vinyl ketone + methacrolein**							**15.09**	1.7 (0.7)
		(1,2)-isoprene hydroxy hydroperoxide								
		(4,3)-isoprene hydroxy hydroperoxide								
		2-butenal	8.50[a]	3.67[a]	3.7	100[std]		22.17		
		cyclobutanone								
		2,3-dihydro-furan								
		2,5-dihydro-furan								
71.086	$C_5H_{10}H^+$	frag. 2-pentanol (88 u)	10.61[b]	1.66[a]	2.27	40[7]	NA	5.39	7.85[x]	2.7 (1.0)
		1-pentene	9.65[a]	0.50[a]	1.9	41[4]	120	4.63		
		Cis-2-pentene	9.84[a]	0.31[b]	1.91	80[1]	106	9.04		
		Trans-2-pentene	9.84[a]	0.11[b]	1.9	42[4]	120	4.83		
		2-methyl-1-butene	9.47[a]	1.32[a]	2.09	44[4]	120	5.46		
		2-methyl-2-butene	10.00[b]	0.21[b]	1.92	44[4]	120	5		
		3-methyl-1-butene	9.38[a]	0.32[a]	1.86	80[1]	106	8.84		
		cyclopentane	9.15[a]	0.00[a]	1.83	34[4]	120	3.69		
		frag. pentanal (86 u)	9.84[a]	2.50[a]	2.82	78[1]	106	13.06		

m/z	Chemical Formula	Tentative Compound Attribution	Polarizability $(10^{-30}\ m^3)$	Dipole moment (Debye)	k_{coll} $(10^{-9}\ cm^3$ $molec^{-1}\ s^{-1})$	PT or fragment yield (%)	E/N (Td)	S_{ind} (tc-ncps $ppbv^{-1}$)	S_{mz} (tc-ncps $ppbv^{-1}$)	LoD (pptv)
		frag. ethyl acetate (88 u) fragments of butyric acid and isobutyric acid	9.16[a]	1.78[a]	2.24	50[std]		6.65		
73.065	$C_4H_8OH^+$	**methyl ethyl ketone (2-butanone)**							**18.03**	2.0 (1.2)
		butanal	8.20[a]	2.72[a]	3.01	65[1]	130	11.72		
		2-methyl-propanal isobutanal, 2-methoxy-1-propene, ethoxy ethene, tetrahydrofuran, 2-butenol	8.24[b]	2.86[a]	3.12	100[12]	0	18.67		
75.044	$C_3H_6O_2H^+$	**hydroxyacetone**			3.50[13]	100[std]		21.15	21.15[z]	1.3 (0.5)
		ethyl formate	7.45[a]	1.93[a]	2.3	95[14]	0	13.23		
		methyl acetate	6.88[a]	1.72[a]	2.11	92[7]	NA	11.73		
		propionic acid	6.90[a]	1.75[a]	2.13	60[15]	135	7.74		
77.023	$C_2H_4O_3H^+$	peracetic acid glycolic acid (= hydroxyacetic acid) frag. peroxyacetic nitric anhydride	6.04[c]	2.40[a]	2.61	10[16]	0	1.58	7.85[u]	2.9 (1.0)
80.058	$^{13}C^{12}C_5H_6H^+$	**benzene isotope**							**0.79**	26 (22)
81.070	$C_6H_8H^+$	**frag. monoterpene (136 u) (sabinene)**							**7.38**	3.8 (1.7)
		alpha-pinene	17.30[17]	0.17[17]	2.39	43.8[18]	120	6.14		
		beta-pinene	17.50[17]	0.74[17]	2.43	42.4[18]	120	6.06		
		limonene	18.30[17]	0.60[17]	2.47	42.4[18]	120	6.16		
		3-carene	17.60[17]	0.17[17]	2.41	33.8[18]	120	4.78		
		myrcene	19.80[17]	0.58[17]	2.57	32.8[18]	120	4.95		
		camphene	17.20[17]	0.67[17]	2.4	36.1[18]	120	5.1		
		alpha-phellandrene	18.67[b]	0.06[b]	2.48	41.5[18]	120	6.05		
		alpha-terpinene			2.50[std]	36.3[18]	120	5.33		

m/z	Chemical Formula	Tentative Compound Attribution	Polarizability (10^{-30} m^3)	Dipole moment (Debye)	k_{coll} (10^{-9} cm^3 molec^{-1} s^{-1})	PT or fragment yield (%)	E/N (Td)	S_{ind} (tc-ncps ppbv^{-1})	S_{mz} (tc-ncps ppbv^{-1})	LoD (pptv)
		gamma-terpinene			2.50[std]	41.3[18]	120	6.07		
		1-hexen-3-yne, 1,3-cyclohexadiene, 1,4-cyclohexadiene, 1-Methyl-3-methylenecyclobutene fragments of hexenol, hexenal, sesquiterpenes								
83.049	$C_5H_6OH^+$	**3-methylfuran**	9.07[c]	1.03[a]	1.92	100[1]	106	11.38	11.18[y]	1.7 (1.0)
		2-methylfuran	9.07[c]	0.65[a]	1.84	100[1]	106	10.98		
83.086	$C_6H_{10}H^+$	**frag. cis-3-hexenol (100 u)**							**7.36**	3.0 (1.1)
		frag. trans-2-hexenol (100 u)			2.5[std]	76[7]	NA	11.16		
		frag. trans-3-hexenol (100 u)			2.5[std]	70[7]	NA	10.28		
		frag. hexanal (100 u)	11.78[a]	2.50[a]	2.84	73[7]	NA	12.17		
		frag. cis-3-hexenyl-acetate (142 u)	16.5[8]	2.00[8]	2.68	61[7]	NA	9.62		
		cyclohexene	10.70[a]	0.33[a]	1.96	100[1]	106	11.5		
		1-hexyne	11.29[b]	1.00[b]	2.1	100[std]		12.35		
		2-hexyne	11.59[b]	0.18[b]	2.03	100[std]		11.93		
		1-methyl-cyclopentane, 1,2-dimethylcyclobutene), 1,3,3-trimethylcyclopropene, 2,3-dimethyl-1,3-butadiene, 2-methyl-1,3-pentadiene, methylene-cyclopentane, cis-1,3-hexadiene, trans-1,3-hexadiene								
85.065	$C_5H_8OH^+$	**E-2-pentenal**	7.37[c]	3.50[a]	3.42	100[12]	0	20.31	20.47[y]	0.8 (0.3)
		E-2-methyl-2-butenal	9.91[c]	3.50[a]	3.61	100[12]	0	21.41		
		cyclopentanone	7.62[19]	3.30[a]	3.32	100[std]		19.68		

m/z	Chemical Formula	Tentative Compound Attribution	Polarizability (10^{-30} m^3)	Dipole moment (Debye)	k_{coll} (10^{-9} cm^3 molec^{-1} s^{-1})	PT or fragment yield (%)	E/N (Td)	S_{ind} (tc-ncps ppbv^{-1})	S_{mz} (tc-ncps ppbv^{-1})	LoD (pptv)
		3-methyl-3-buten-2-one, 3-penten-2-one, 1-penten-3-one, (2E)-2-methylbut-2-enal, 2-methyl-(Z)-2-butenal, 4-methyl-2,3-dihydrofuran, 1-cyclopropyl-ethanone, 2,3-dihydro-5-methyl-furan, 3-methyl-2-butenal fragments of levoglucosan and pentanoic acid								
85.101	C$_6$H$_{12}$H$^+$	**frag. hexanol (102 u)**	12.04[b]	1.60[a]	2.31	29[7]	NA	3.94	3.94[z]	3.8 (1.4)
		1-hexene	11.70[a]	0.40[a]	2.05	100[20]	0	12.02		
		E-2-hexene	11.53[a]	0.05[a]	2.02	27[4]	120	3.21		
		2-methyl-2-pentene			2.50[std]	29[4]	120	4.26		
		cyclohexane	10.9[a]	0.00[a]	1.96	15[4]	120	1.73		
		methylcyclopentane	10.78[a]	0.11[b]	1.96	28[4]	120	3.22		
		trans-4-methyl-2-pentene			2.50[std]	31[4]	120	4.55		
		fragments of 2,3-dimethyl-2-butene, 2-methyl-1-pentene, (Z)-2-hexene, hexyl acetate								
87.044	C$_4$H$_6$O$_2$H$^+$	**2,3-butanedione**	8.20[a]	0.00[a]	1.7	93[7]	NA	9.46	7.85[x]	3.0 (1.2)
		y-butyrolactone	7.96[b]	3.00[17]	3.13	100[21]	0	18.75		
		cyclopropane carboxylic acid	10.00[21]	1.80[a]	2.32	90[21]	0	12.47		

m/z	Chemical Formula	Tentative Compound Attribution	Polarizability (10^{-30} m^3)	Dipole moment (Debye)	k_{coll} (10^{-9} cm^3 molec^{-1} s^{-1})	PT or fragment yield (%)	E/N (Td)	S_{ind} (tc-ncps ppbv^{-1})	S_{mz} (tc-ncps ppbv^{-1})	LoD (pptv)
		methyl acrylate, 2,3-dihydro-1,4-dioxin, methyl acrylate, methacrylic acid, vinyl acetate, crotonic acid, isocrotonic acid, **acetic acid ethenyl ester, 2-propenoic acid methyl ester, 4-hydroxy-2-butenal**								
87.080	C$_5$H$_{10}$OH$^+$	**pentanal**	9.84[a]	2.50[a]	2.83	22[1] 5[7]	106 NA	3.7 0.84	7.85[x]	1.7 (0.6)
		3-methylbutanal	10[12]	2.50[a]	2.84	70[12]	0	11.78		
		allyl ethyl ether	10.7[21]	1.20[a]	2.1	75[21]	0	9.34		
		2-methyl-3-buten-1-ol			2.50[std]	19[1]	106	2.81		
		2-pentanone	9.93[a]	2.70[a]	3	92[7]	NA	16.39		
		3-pentanone	9.93[a]	2.82[a]	3.1	100[1]	106	18.39		
		2-methyl-3-buten-2-ol	10.50[23]	1.51[23]	2.2	19[22]	135	2.48		
		1-penten-3-ol	10.60[23]	1.43[23]	2.17	7.5[22]	135	0.96		
		3-methyl-3-buten-1-ol, 3-methyl-2-buten-1-ol, **(E)-2-penten-1-ol**, (Z)-2-penten-1-ol, 2-methylbutanal, 3-methyl-2-butanone, tetrahydro-2-methyl-furan, tetrahydropyran								
89.023	C$_3$H$_4$O$_3$H$^+$	**pyruvic acid** 1,3-dioxolan-2-one	7.25[c]	2.30[a]	2.55	80[21]	0	12.35	12.35[z]	1.7 (0.7)
89.060	C$_4$H$_8$O$_2$H$^+$	**1,4-dioxane**	9.30[a]	0.00[a]	1.81	80[3]	130	8.65	7.85[x]	1.9 (0.7)
		1,3-dioxane	8.46[b]	1.98[b]	2.34	100[std]		14		
		3-hydroxybutanone (=acetoin)	8.89[c]	2.60[a]	2.87	100[21]	0	17.18		
		methyl propanoate	8.97[a]	1.80[a]	2.24	100[24]	120	13.44		

m/z	Chemical Formula	Tentative Compound Attribution	Polarizability (10^{-30} m^3)	Dipole moment (Debye)	k_{coll} (10^{-9} cm^3 molec^{-1} s^{-1})	PT or fragment yield (%)	E/N (Td)	S_{ind} (tc-ncps ppbv^{-1})	S_{mz} (tc-ncps ppbv^{-1})	LoD (pptv)
		ethyl acetate	9.16[a]	1.78[a]	2.24	7[24]	135	0.94		
		butanoic acid	8.58[a]	1.65[a]	2.13	95[14]	0	12.1		
		isobutanoic acid	8.89[c]	1.08[a]	1.91	90[14]	0	10.27		
		tetrahydrofuran-3-ol, **formic acid 1-methylethyl ester**, 1,1-dimethoxy-ethene, methylethyl formate, propyl formate, methyl ester propanoic acid, 1-hydroxy-3-butanone								
93.070	C$_7$H$_8$H$^+$	**toluene**							**12.02**	1.5 (0.7)
		frag. p-cymene (134 u)	17[25]	0[25]	2.37	90[25]	135	12.4		
		2,5-norbornadiene, 1,5-heptadiyne								
95.086	C$_7$H$_{10}$H$^+$	1,3-cycloheptadiene 2-norbornene fragments of monoterpenes and sesquiterpenes							7.85[u]	2.4 (0.9)
97.028	C$_5$H$_4$O$_2$H$^+$	**2-furfural**	10.87[a]	3.54[a]	3.64	100[std]		21.58	21.58[z]	0.9 (0.3)
		3-furfural	10.87[a]	3.54[a]	3.64	100[std]		21.58		
		2-furancarboxaldehyde (=2-furfural) cyclopentadione o-oxide								
97.065	C$_6$H$_8$OH$^+$	**2,4-hexadienal**, 2-ethylfuran, 2,5-dimethylfuran, 2,4-dimethylfuran, 3,4-dimethylfuran, 7-Oxa-bicyclo[2.2.1]hept-2-ene							7.85[u]	2.0 (1.0)
97.101	C$_7$H$_{12}$H$^+$	**frag. heptanal (114 u)**	13.52[a]	2.50[a]	2.87	65[7]	NA	10.85	11.51[y]	1.6 (0.6)
		cycloheptene	12.59[b]	0.27[b]	2.09	100[std]		12.17		

m/z	Chemical Formula	Tentative Compound Attribution	Polarizability (10^{-30} m^3)	Dipole moment (Debye)	k_{coll} (10^{-9} cm^3 molec^{-1} s^{-1})	PT or fragment yield (%)	E/N (Td)	S_{ind} (tc-ncps ppbv^{-1})	S_{mz} (tc-ncps ppbv^{-1})	LoD (pptv)
		1-methylcyclohexene, 1,2-dimethyl-cyclopentene								
99.044	C$_5$H$_6$O$_2$H$^+$	**furfuryl alcohol** 3-methyl-2-furanone, 4-Methyl-5H-furan-2-one	9.79[c]	1.92[a]	2.34	100[std]		13.88	13.88[z]	1.5 (0.8)
99.080	C6H10OH+	**E-2-hexenal**	12.57[b]	4.45[b]	4.32	100[26]	0	25.41	7.85[x]	1.9 (0.8)
		Z-3-hexenal	12.01[b]	2.79[b]	3.1	35[26]	0	6.38		
		cyclohexanone methyl cyclopentanone E-3-hexenal, Z-2-hexenal, 3-methyl-3-penten-2-one, 3-hexen-2-one, 4-methyl-3-penten-2-one, 7-oxabicyclo[2.2.1]heptane, cyclohexene oxide								
101.023	C$_4$H$_4$O$_3$H$^+$	Succinic anhydride							7.85[u]	2.6 (0.9)
101.060	C$_5$H$_8$O$_2$H$^+$	**C5-hydroxycarbonyl / ISOPOOH**							7.85[u]	2.3 (0.9)
		4-oxopentanal	9.73[27]	2.95[27]	3.14	100[std]		18.61		
		y-valerolactone			2.50[std]	100[28]	0	14.83		
		1,5-pentanedial	10.21[b]	3.68[b]	3.68	50[29]	0	10.93		
		acetylacetone	10.36[b]	1.49[b]	2.15	100[std]		12.74		

m/z	Chemical Formula	Tentative Compound Attribution	Polarizability $(10^{-30}$ m$^3)$	Dipole moment (Debye)	k_{coll} $(10^{-9}$ cm^3 molec^{-1} s$^{-1})$	PT or fragment yield (%)	E/N (Td)	S_{ind} (tc-ncps ppbv^{-1})	S_{mz} (tc-ncps ppbv^{-1})	LoD (pptv)
		methyl methacrylate, 2,3-pentanedione, 3-methyl-2-butenoic acid, methyl isocrotonate, 2-methyl-(Z)-2-butenoic acid, 2-methyl-(E)-2-butenoic acid, ethyl acrylate, cyclobutylcarboxylic acid, methyl cyclopropanecarboxylate, 3-pentenoic acid								
101.096	C$_6$H$_{12}$OH$^+$	**n-hexanal**	11.78[a]	2.94[b]	3.21	5[7] 43[1]	NA 106	0.94 8.11	7.85[x]	1.4 (0.5)
		cis-3-hexen-1-ol	12.6[23]	1.65[23]	2.37	1[7] 0[22]	NA 135	0.14 0		
		trans-2-hexen-1-ol	12.6[23]	1.45[23]	2.29	0.2[7] 0[22]	NA 135	0.03 0		
		2-hexanone	11.85[c]	2.66[a]	2.98	100[1]	106	17.49		
		3-hexanone	11.85[c]	2.80[a]	3.1	100[std]		18.2		
		cyclohexanol	11.32[b]	1.51[b]	2.23	100[std]		13.07		
		2,2-dimethyltetrahydrofuran, 3,3-dimethyl-2-butanone, oxepane, isobutylmethylketone								
103.039	C$_4$H$_6$O$_3$H$^+$	**acetic anhydride** propylene carbonate (GL)	8.90[a]	2.80[a]	2.98	100[std]		17.84	17.84[z]	0.8 (0.4)
103.075	C$_5$H$_{10}$O$_2$H$^+$	**methyl butanoate**	10.40[a]	1.80[a]	2.3	98[24]	140	13.35	7.85[x]	1.5 (0.5)
		n-propyl acetate	10.72[c]	1.78[a]	2.31	3[7]	NA	0.41		
		pentanoic acid (=valeric acid)	10.72[c]	1.61[a]	2.22	90[14]	0	11.87		
		butyl formate	10.72[c]	2.03[a]	2.45	2[24]	120	0.29		
		ethyl propanoate	10.40[a]	1.74[a]	2.26	37[7]	NA	4.97		
		Trimethylacetic acid	10.72[c]	1.80[a]	2.32	90[14]	0	12.37		

m/z	Chemical Formula	Tentative Compound Attribution	Polarizability (10^{-30} m^3)	Dipole moment (Debye)	k_{coll} (10^{-9} cm^3 molec^{-1} s^{-1})	PT or fragment yield (%)	E/N (Td)	S_{ind} (tc-ncps ppbv^{-1})	S_{mz} (tc-ncps ppbv^{-1})	LoD (pptv)
		1,2-cyclopentanediol **C5-diol**, 3-methyl-butanoic acid (=isovaleric acid), 2-methyl-butanoic acid, 2,2-dimethyl propanoic acid (= pivalic acid), 4-hydroxy-3-methyl-2-butanone, **acetic acid methylethyl ester (= isopropyl acetate), 2-methylpropanoic acid methyl ester (=2-methylpropyl ester), 1-hydroxy-2-methyl-3-butanone, 1-hydroxy-3-methyl-2-butanone, 5-hydroxy-2-pentanone**	10.62[c]	3.31[a]	3.44	2[29]	0	0.41		
104.049	C$_7$H$_5$NH$^+$	benzonitrile isocyanobenzene	12.5[a]	4.18[a]	4.13	100[std]		24.03	24.03[z]	0.41 (0.19)
107.086	C$_8$H$_{10}$H$^+$	**m-xylene** **o-xylene** **p-xylene** ethyl benzene 1,3-dimethyl-benzene **frag. monoterpene (136 u)**	14.50[a] 14.30[a] 14.20[a]	0.64[a] 0.00[a] 0.59[a]	2.25 2.21 2.22	100[std] 100[std] 82[4]	120	12.97 12.73 10.61	**12.7**	1.3 (0.8)
111.117	C$_8$H$_{14}$H$^+$	**frag. octanal (128 u)** 4-methyl-1,3-heptadiene, 1,3-octadiene frag. monoterpene oxidation product	15.48[a]	2.50[a]	2.92	40[7]	NA	6.74	7.85[u]	2.1 (0.8)

m/z	Chemical Formula	Tentative Compound Attribution	Polarizability (10^{-30} m^3)	Dipole moment (Debye)	k_{coll} (10^{-9} cm^3 molec^{-1} s^{-1})	PT or fragment yield (%)	E/N (Td)	S_{ind} (tc-ncps ppbv^{-1})	S_{mz} (tc-ncps ppbv^{-1})	LoD (pptv)
115.075	C$_6$H$_{10}$O$_2$H$^+$	2,5-hexanedione, ethyl-2-butanoate, cyclopentylcarboxylic acid, 3,5-dimethyloxolan-2-one							7.85[u]	2.0 (1.0)
115.112	C$_7$H$_{14}$OH$^+$	**2-heptanone**	13.70[c]	2.59[a]	2.94	100[7]	NA	17.11	7.85[x]	1.3 (0.5)
		3-heptanone	13.70[c]	2.78[a]	3.09	100[7]	NA	17.96		
		2,4-dimethyl-3-pentanone	13.50[a]	2.74[a]	3.05	100[std]		17.74		
		heptanal	13.52[a]	2.50[a]	2.87	5[7]	NA	0.83		
		4-heptanone, **5-methyl-2-hexanone**, 1-methoxycyclohexane, cyclohexanemethanol								
117.055	C$_5$H$_8$O$_3$H$^+$	methyl acetoacetate, 4-hydroxy-2-methylbut-2-enoic acid (=4-hydroxytiglic acid), 4-oxo-pentanoic acid (=levulinic acid), **1-acetyloxy-2-propanone**							7.85[u]	1.7 (1.0)
117.091	C$_6$H$_{12}$O$_2$H$^+$	ethyl butanoate	12.55[c]	1.74[a]	2.38	58[7]	NA	8.1	7.85[x]	1.5 (0.7)
						14[24]	140	1.96		
						55[24]	120	7.68		
		ethyl isobutanoate			2.50[std]	60[24]	120	8.82		
		methyl 2-methylbutanoate			2.50[std]	91[24]	120	13.37		
		propyl propanoate			2.50[std]	25[24]	120	3.67		
		butyl acetate	12.55[c]	1.87[a]	2.44	9[7]	NA	1.29		
		ethyl-2-methyl-propanoate, hexanoic acid (= caproic acid), 4-hydroxy-4-methyl-2-pentanone, cis-1,3-cyclohexanediol, trans-1,3-cyclohexanediol								

m/z	Chemical Formula	Tentative Compound Attribution	Polarizability (10^{-30} m^3)	Dipole moment (Debye)	k_{coll} (10^{-9} cm^3 molec^{-1} s^{-1})	PT or fragment yield (%)	E/N (Td)	S_{ind} (tc-ncps ppbv^{-1})	S_{mz} (tc-ncps ppbv^{-1})	LoD (pptv)
121.101	C$_9$H$_{12}$H$^+$	**1,2,4-trimethylbenzene**							**13.79**	1.0 (0.4)
		1,2,3-trimethylbenzene	17.09[a]	0.60[a]	2.41	100[1]	106	13.78		
		1,3,5-trimethylbenzene	15.80[a]	0.00[a]	2.3	100[1]	106	13.14		
		n-propyl benzene (=isocumene)	15.94[c]	0.60[a]	2.33	91[1]	106	12.12		
		2-ethyltoluene (=o-ethyltoluene)			2.50[std]	97[4]	120	13.86		
		3-ethyltoluene			2.50[std]	96[4]	120	13.72		
		4-ethyltoluene			2.50[std]	94[4]	120	13.44		
		isopropylbenzene (=cumene)	17.20[b]	0.79[b]	2.44	44[1]	106	6.13		
						21[4]	120	2.93		
		frag. sesquiterpene (204 u)								
123.044	C$_7$H$_6$O$_2$H$^+$	**benzoic acid**	13.54[b]	2.19[b]	2.65	100[std]		15.44	15.44[z]	0.8 (0.4)
		o-hydroxybenzaldehyde								
123.080	C$_8$H$_{10}$OH$^+$	2-phenylethanol	14.72[c]	1.50[a]	2.42	100[32]	0	13.94	13.94[y]	0.8 (0.3)
		1-phenylethanol	14.72[c]	1.50[a]	2.42	100[32]	0	13.94		
		4-ethylphenol	14.72[c]	1.50[a]	2.42	100[32]	0	13.94		
		methyl anisole								
		methoxymethyl benzene								
123.117	C$_9$H$_{14}$H$^+$	apopinene							7.85[u]	1.8 (0.9)
		santene								
		2-norbornene								
129.127	C$_8$H$_{16}$OH$^+$	**1-octen-3-ol**	16.20[23]	1.38[23]	2.47	8[22]	135	1.14	7.85[x]	1.4 (0.5)
						6[7]	NA	0.85		
		octanal	15.48[b]	2.54[b]	2.94	11[7]	NA	1.87		
		2-octanone	15.54[c]	2.70[a]	3.05	100[7]	NA	17.61		
		3-octanone			2.50[std]	100[7]	NA	14.42		
		octanone,								
		2,2,4-trimethyl-3-pentanone								
133.101	C$_{10}$H$_{12}$H$^+$	**p-cymenene**							7.85[u]	2 (2)
		methyl propenyl benzene								

m/z	Chemical Formula	Tentative Compound Attribution	Polarizability $(10^{-30}$ m$^3)$	Dipole moment (Debye)	k_{coll} $(10^{-9}$ cm^3 molec^{-1} s$^{-1})$	PT or fragment yield (%)	E/N (Td)	S_{ind} (tc-ncps ppbv^{-1})	S_{mz} (tc-ncps ppbv^{-1})	LoD (pptv)
		1,2,3,4-tetrahydronaphthalene			2.50^{std}	100^4	120	14.16		
		ethyl styrene,								
		1-butenylbenzene,								
		2,3-dihydro-4-methyl-indene,								
		isopropenyltoluene,								
		1-cyclopropyl-2-methylbenzene,								
		1-cyclopropyl-3-methylbenzene,								
		2-methylprop-2-enylbenzene,								
		1-cyclopropyl-4-methylbenzene,								
		1-methyl-2-(1-methylethenyl)-benzene,								
		1-methyl-3-(1-methylethenyl)benzene								
135.117	$C_{10}H_{14}H^+$	**p-cymene**	17^{25}	0^{25}	2.37	10^{25}	135	1.34	1.34^z	9 (4)
		1,4-diethylbenzene			2.50^{std}	96^4	120	13.6		
		1,2-diethylbenzene			2.50^{std}	100^1	106	14.16		
		1,3-diethylbenzene			2.50^{std}	100^1	106	14.16		
		(n)-butylbenzene			2.50^{std}	95^1	106	13.46		
		sec-butylbenzene			2.50^{std}	11^4	120	1.56		
		tert-butylbenzene			2.50^{std}	50^1	106	7.08		
		1,2,4,5-tetramethylbenzene			2.50^{std}	100^1	106	14.16		
		1,2,3,5-tetramethylbenzene (= isodurene), m-cymene,								
		2-ethyl-p-xylene,								
		isobutylbenzene,								
		methyl-n-propylbenzene,								
		p-mentha-1,5,8-triene								
		frag. alpha-pinene oxide								
137.060	$C_8H_8O_2H^+$	methyl benzoic acid							7.85^u	1.8 (1.3)
		methyl benzoate			2.50^{std}	90^{14}	0	12.86		

m/z	Chemical Formula	Tentative Compound Attribution	Polarizability (10^{-30} m^3)	Dipole moment (Debye)	k_{coll} (10^{-9} cm^3 molec^{-1} s^{-1})	PT or fragment yield (%)	E/N (Td)	S_{ind} (tc-ncps ppbv^{-1})	S_{mz} (tc-ncps ppbv^{-1})	LoD (pptv)
		4' -hydroxyacetophenone, 3-methoxybenzaldehyde, 4-methoxybenzaldehyde, m-acetylphenol,								
137.132	C$_{10}$H$_{16}$H$^+$	**monoterpenes** (sabinene)							**8.36**	2.3 (1.1)
		alpha-pinene	17.30[17]	0.17[17]	2.39	54.9[18]	120	7.36		
		beta-pinene	17.50[17]	0.74[17]	2.43	56.1[18]	120	7.66		
		limonene	18.30[17]	0.60[17]	2.47	52.8[18]	120	7.33		
		3-carene	17.60[17]	0.17[17]	2.41	65.0[18]	120	8.79		
		myrcene	19.80[17]	0.58[17]	2.57	55.4[18]	120	7.99		
		camphene	17.20[17]	0.67[17]	2.4	62.0[18]	120	8.49		
		alpha-phellandrene	18.67[b]	0.06[b]	2.48	57.3[18]	120	7.54		
		alpha-terpinene			2.5[std]	62.9[18]	120	8.99		
		gamma-terpinene			2.5[std]	58.8[18]	120	8.4		
		terpinolene, trans-b-ocimene, gamma terpinene, d-limonene, cis-b-ocimene, a-thujene, c-carene, 3-methylene-1,5,5-trimethylcyclohexene								
		frag. linalool (154 u)	20.00[8]	1.54[8]	2.71	49.5[18]	120	7.54		
139.021	C$_7$H$_6$OSH$^+$	benzenecarbothioic acid							7.85[u]	1.7 (0.8)
139.112	C$_9$H$_{14}$OH$^+$	**nopinone**	15.70[33]	3.50[33]	3.67	97[33]	0	20.18	18.98[y]	0.7 (0.4)
						88[34]	NA	18.31		
		4-acetyl-1-methyl-cyclohexene	16.30[33]	2.90[33]	3.2	98[33]	0	17.78		
		Other monoterpene oxidation products: 4-acetyl-2-cyclohexene, **sabinaketone, camphenilone** isophorone								

m/z	Chemical Formula	Tentative Compound Attribution	Polarizability $(10^{-30}$ m$^3)$	Dipole moment (Debye)	k_{coll} $(10^{-9}$ cm^3 molec^{-1} s$^{-1})$	PT or fragment yield (%)	E/N (Td)	S_{ind} (tc-ncps ppbv^{-1})	S_{mz} (tc-ncps ppbv^{-1})	LoD (pptv)
		3,5,5-trimethyl-3-cyclohexene-1-one (=beta-isophorone) 2-pentylfuran								
141.127	C$_9$H$_{16}$OH$^+$	trans-2-nonenal 3,6-nonadienol 3-nonen-2-one cyclononanone	17.15[c]	3.50[a]	3.71	100[12]	0	20.99	7.85[u]	1.5 (1.1)
143.107	C$_8$H$_{14}$O$_2$H$^+$	**(Z)-3-hexenyl acetate** 2,3-octanedione methyl cyclohexanoate	16.5[8]	2.00[8]		2[7]	NA	0.31	7.85[u]	1.8 (1.2)
143.143	C$_9$H$_{18}$OH$^+$	**Nonanal** 2-nonanone Hexamethylacetone 5-Nonanone	17.41[b] 17.34[c]	2.84[b] 2.80[a]	3.19 3.16	19[7] 100[7]	NA NA	3.43 17.91	7.85[x]	1.2 (0.4)
149.132	C$_{11}$H$_{16}$H$^+$	**frag. sesquiterpene (204 u)** beta-caryophyllene alpha-humulene longifolene alpha-cedrene 4-tert-butyltoluene 1-ethyl-2-propylbenzene neopentylbenzene	26.60[30] 27.40[30] 25.90[30] 25.30[30]	0.65[30] 0.24[30] 0.94[30] 0.21[30]	2.91 2.94 2.9 2.83	11[31] 8[31] 11[31] 4.5[31]	135 135 135 135	1.78 1.31 1.78 0.71	1.40[y]	9 (7)
151.112	C$_{10}$H$_{14}$OH$^+$	**frag. pinonaldehyde (168 u)** **frag. coronaldehyde (168 u)** p-cymen-8-ol **o-thymol** **m-thymol** carvone d-verbenone eucarvone	17.90[33] 18.10[33]	2.26[33] 3.58[33]	2.84 3.74	60[33] 22[33]	0 0	9.58 4.62	7.10[y]	2.0 (1.3)

m/z	Chemical Formula	Tentative Compound Attribution	Polarizability $(10^{-30}$ m^3)	Dipole moment (Debye)	k_{coll} $(10^{-9}$ cm^3 molec^{-1} s^{-1})	PT or fragment yield (%)	E/N (Td)	S_{ind} (tc-ncps ppbv^{-1})	S_{mz} (tc-ncps ppbv^{-1})	LoD (pptv)
		carvol								
153.055	C$_8$H$_8$O$_3$H$^+$	**methyl salicylate** vanillin methyl m-hydroxybenzoate 3,4-dihydroxyacetophenone p-anisic acid	15.82[9]	2.53[9]	2.91	100[9]	0	16.64	16.64[z]	0.7 (0.4)
153.127	C$_{10}$H$_{16}$OH$^+$	**camphor** trans-2,4-decadienal alpha pinene oxide fenchone 2-methyl-5-(1-methylethenyl)-2-cyclohexen-1-ol (=carveol) p-menth-1-en-3-one (= 1-terpineol) E)-3(10)-caren-4-ol 2-carene epoxide)	17.20[8] 18.76[c] 17.30[33]	3.28[8] 3.50[a] 1.99[33]	3.5 3.72 2.71	100[8] 100[12] 11[33]	0 0 0	19.64 20.86 1.67	19.64[z]	0.6 (0.3)
155.107	C$_9$H$_{14}$O$_2$H$^+$	norpinonaldehyde **arbusculone** **C9 unsaturated esters** 5,5-dimethyl-3-methoxycyclohex-2-enone							7.85[u]	1.7 (0.9)
157.122	C$_9$H$_{16}$O$_2$H$^+$	(4R,5R)-5-butyl-4-methyldihydrofuran-2(3H)-one (=(Z)-whiskey lactone)							7.85[u]	1.6 (0.7)
167.107	C$_{10}$H$_{14}$O$_2$H$^+$	wine lactone frag. cis-pinonic acid piperitenone oxide carvone oxide							7.85[u]	1.7 (0.8)
169.122	C$_{10}$H$_{16}$O$_2$H$^+$	**pinonaldehyde** **caronaldehyde**	17.90[33] 18.10[33]	2.26[33] 3.58[33]	2.84 3.74	7[33] 13[33]		1.12 2.73	1.93[y]	7 (4)

m/z	Chemical Formula	Tentative Compound Attribution	Polarizability (10^{-30} m^3)	Dipole moment (Debye)	k_{coll} (10^{-9} cm^3 molec^{-1} s^{-1})	PT or fragment yield (%)	E/N (Td)	S_{ind} (tc-ncps ppbv^{-1})	S_{mz} (tc-ncps ppbv^{-1})	LoD (pptv)
205.195	C$_{15}$H$_{24}$H$^+$	**sesquiterpenes**							7.96[y]	2.3 (1.1)
		beta-caryophyllene	26.60[30]	0.65[30]	2.91	31[31]		4.81		
		alpha-humulene	27.40[30]	0.24[30]	2.94	47[31]		7.37		
		longifolene	25.90[30]	0.94[30]	2.9	61[31]		9.42		
		alpha-cedrene	25.30[30]	0.21[30]	2.83	68[31]		10.24		
		valencene, germacrene, amorphene, gamma-bisabolene, bourbonene, copaene, cubenene, farnesene, gurjunene, longipinene, muurolene, cadinene, elemene, humulene, bergamotene,								

[*] The sensitivity for formaldehyde was determined through comparison of PTR-ToF-MS signal at m/z 31.018 (in tc-ncps) with formaldehyde measurements acquired in the nearby ISSeP station in the framework of the EMEP intensive measurement period in the summer of 2022 (Fagerli et al., 2023).

[a] Information found in the PTR-library database (Pagonis et al., 2019)

[b] Cappellin et al. (2012)

[c] Polarizability calculated using the empirical method of Miller and Savchik (1979)

[x] A standard sensitivity of 7.85 tc-ncps/ppbv, corresponding to a H$_3$O$^+$/VOC collision rate constant of 2.5×10^{-9} cm^3 molecule^{-1} s^{-1} and a proton transfer yield of 50%, was used because of the large range variability of calculated

sensitivities for individual compounds at this m/z

[y] Average of the calculated sensitivities for the potentially contributing compounds due to limited variability

[z] The calculated sensitivity of the compound which is expected to contribute most in this kind of environment is considered

[u] A standard sensitivity of 7.85 tc-ncps/ppbv was used by lack of better estimated calibration factors or by lack of knowledge of which compound is expected to contribute most to the m/z ion signal in this type of environment.

[1] Warneke et al. (2003)

[2] Mean fragmentation fraction obtained from the calibration or the ambient spectra. The standard deviation of the fragment fraction is noted between parenthesis.

[3] Lindinger et al. (1998)

[4] Gueneron et al. (2015)

[5] Sekimoto et al. (2017)

[6] Crespo González (2012)

[7] Buhr et al. (2002)

[8] Amelynck et al. (2005)

[9] Sovová et al. (2011)

[10] Haase et al. (2012)

[11] Španěl et al. (2002b)

[12] Španěl et al. (2002a)

[13] Karl et al. (2009)

[14] Španěl and Smith (1998)

[15] Meurs et al. (2022)

[16] Španěl et al. (2003)

[17] Schoon et al. (2003)

[18] Tani et al. (2003)

[19] Johnson (2002)

[20] Diskin et al. (2002)

[21] Smith et al. (2011)

[22] Demarcke et al. (2010)

[23] Schoon et al. (2007)

[24] Aprea et al. (2007)

[25] Tani et al. (2003)

[26] Španěl et al. (1995)

[27] Salthammer et al. (2023)

[28] Wang et al. (2004a)

[29] Španěl et al. (1997)

[30] Dhooghe et al. (2008)

[31] Demarcke et al. (2009)

[32] Wang et al. (2004b)

[33] Schoon et al. (2004)

[34] Wisthaler et al. (2001)

References

Amelynck, C., Schoon, N., Kuppens, T., Bultinck, P., and Arijs, E.: A selected ion flow tube study of the reactions of H3O+, NO+ and O2+ with some oxygenated biogenic volatile organic compounds, International Journal of Mass Spectrometry, 247, 1–9, https://doi.org/10.1016/j.ijms.2005.08.010, 2005.

Aprea, E., Biasioli, F., Märk, T. D., and Gasperi, F.: PTR-MS study of esters in water and water/ethanol solutions: Fragmentation patterns and partition coefficients, International Journal of Mass Spectrometry, 262, 114–121, https://doi.org/10.1016/j.ijms.2006.10.016, 2007.

Aubinet, M., Feigenwinter, C., Heinesch, B., Laffineur, Q., Papale, D., Reichstein, M., Rinne, J., and Van Gorsel, E.: Nighttime Flux Correction, pp. 133–157, Springer Netherlands, Dordrecht, ISBN 978-94-007-2351-1, https://doi.org/10.1007/978-94-007-2351-1_5, 2012.

Aubinet, M., Hurdebise, Q., Chopin, H., Debacq, A., De Ligne, A., Heinesch, B., Manise, T., and Vincke, C.: Inter-annual variability of Net Ecosystem Productivity for a temperate mixed forest: A predominance of carry-over effects?, Agricultural and Forest Meteorology, 262, 340–353, https://doi.org/10.1016/j.agrformet.2018.07.024, 2018.

Bachy, A., Aubinet, M., Amelynck, C., Schoon, N., Bodson, B., Moureaux, C., Delaplace, P., De Ligne, A., and Heinesch, B.: Methanol exchange dynamics between a temperate cropland soil and the atmosphere, Atmospheric Environment, 176, 229–239, https://doi.org/10.1016/j.atmosenv.2017.12.016, 2018.

Buhr, K., Van Ruth, S., and Delahunty, C.: Analysis of volatile flavour compounds by Proton Transfer Reaction-Mass Spectrometry: fragmentation patterns and discrimination between isobaric and isomeric compounds, International Journal of Mass Spectrometry, 221, 1–7, https://doi.org/10.1016/S1387-3806(02)00896-5, 2002.

Cappellin, L., Karl, T., Probst, M., Ismailova, O., Winkler, P. M., Soukoulis, C., Aprea, E., Märk, T. D., Gasperi, F., and Biasioli, F.: On Quantitative Determination of Volatile Organic Compound Concentrations Using Proton Transfer Reaction Time-of-Flight Mass Spectrometry, Environmental Science & Technology, 46, 2283–2290, https://doi.org/10.1021/es203985t, 2012.

Crespo González, E.: Proton transfer reaction-mass spectrometry, applications in life sciences, PhD dissertation, Radboud Universiteit Nijmegen, Nijmegen, https://hdl.handle.net/2066/94176, 2012.

de Gouw, J. and Warneke, C.: Measurements of volatile organic compounds in the earth's atmosphere using proton-transfer-reaction mass spectrometry, Mass Spectrometry Reviews, 26, 223–257, https://doi.org/10.1002/mas.20119, 2007.

Demarcke, M., Amelynck, C., Schoon, N., Dhooghe, F., Van Langenhove, H., and Dewulf, J.: Laboratory studies in support of the detection of sesquiterpenes by proton-transfer-reaction-mass-spectrometry, International Journal of Mass Spectrometry, 279, 156–162, https://doi.org/10.1016/j.ijms.2008.10.023, 2009.

Demarcke, M., Amelynck, C., Schoon, N., Dhooghe, F., Rimetz-Planchon, J., Van Langenhove, H., and Dewulf, J.: Laboratory studies in support of the detection of biogenic unsaturated alcohols by proton transfer reaction-mass spectrometry, International Journal of Mass Spectrometry, 290, 14–21, https://doi.org/10.1016/j.ijms.2009.11.005, 2010.

Dhooghe, F., Amelynck, C., Schoon, N., Debie, E., Bultinck, P., and Vanhaecke, F.: A selected ion flow tube study of the reactions of H3O+, NO+ and O2+ with a series of sesquiterpenes, International Journal of Mass Spectrometry, 272, 137–148, https://doi.org/10.1016/j.ijms.2008.02.002, 2008.

Diskin, A. M., Wang, T., Smith, D., and Španěl, P.: A selected ion flow tube (SIFT), study of the reactions of H3O+, NO+ and O2+ ions with a series of alkenes; in support of SIFT-MS, International Journal of Mass Spectrometry, 218, 87–101, https://doi.org/10.1016/S1387-3806(02)00662-0, 2002.

Dusanter S., Holzinger R., Klein F., Salameh T., and Jamar M.: Measurement Guidelines for VOC Analysis by PTR-MS, https://www.actris.eu/sites/default/files/inline-files/PTRMS%20SOP%20%28April2025%29.pdf, 2025.

Ester, M., Kriegel, H.-P., Sander, J., and Xu, X.: A Density-Based Algorithm for Discovering Clusters in Large Spatial Databases with Noise, www.aaai.org, 1996.

Fagerli, H., Benedictow, A., Van Caspel, W., Gauss, M., Ge, Y., Jonson, J. E., Klein, H., Nyíri, Á., Simpson, D., Tsyro, S., Valdebenito, Á., Wind, P., Aas, W., Hjellbrekke, A., Solberg, S., Tørseth, K., Espen Yttri, K., Matthews, B., Schindlbacher, S., Ullrich, B., Wankmüller, R., Klimont, Z., Scheuschner, T., Kuenen, J. J. P., Hellén, H., Jaffrezo, J.-L., Tusha, D., Mothes, F., Salameh, T., van Drooge, B. L., and Wegener, R.: EMEP Status report: Transboundary particulate matter, photo-oxidants, acidifying and eutrophying components, Tech. rep., Norwegian Meteorological Institute, ISSN 1504-6192, https://emep.int/publ/reports/2023/EMEP_Status_Report_1_2023.pdf, 2023.

Finco, A., Coyle, M., Nemitz, E., Marzuoli, R., Chiesa, M., Loubet, B., Fares, S., Diaz-Pines, E., Gasche, R., and Gerosa, G.: Characterization of ozone deposition to a mixed oak–hornbeam forest – flux measurements at five levels above and inside the canopy and their interactions with nitric oxide, Atmospheric Chemistry and Physics, 18, 17 945–17 961, https://doi.org/10.5194/acp-18-17945-2018, 2018.

Gueneron, M., Erickson, M. H., VanderSchelden, G. S., and Jobson, B. T.: PTR-MS fragmentation patterns of gasoline hydrocarbons, International Journal of Mass Spectrometry, 379, 97–109, https://doi.org/10.1016/j.ijms.2015.01.001, 2015.

Guenther, A. B., Jiang, X., Heald, C. L., Sakulyanontvittaya, T., Duhl, T., Emmons, L. K., and Wang, X.: The Model of Emissions of Gases and Aerosols from Nature version 2.1 (MEGAN2.1): an extended and updated framework for modeling biogenic emissions, Geoscientific Model Development, 5, 1471–1492, https://doi.org/10.5194/gmd-5-1471-2012, 2012.

Haase, K. B., Keene, W. C., Pszenny, A. A. P., Mayne, H. R., Talbot, R. W., and Sive, B. C.: Calibration and intercomparison of acetic acid measurements using proton-transfer-reaction mass spectrometry (PTR-MS), Atmospheric Measurement Techniques, 5, 2739–2750, https://doi.org/10.5194/amt-5-2739-2012, 2012.

Hellén, H., Praplan, A. P., Tykkä, T., Ylivinkka, I., Vakkari, V., Bäck, J., Petäjä, T., Kulmala, M., and Hakola, H.: Long-term measurements of volatile organic compounds highlight the importance of sesquiterpenes for the atmospheric chemistry of a boreal forest, Atmospheric Chemistry and Physics, 18, 13 839–13 863, https://doi.org/10.5194/acp-18-13839-2018, 2018.

Johnson, R.: Computational Chemistry Comparison and Benchmark Database, NIST Standard Reference Database 101, https://doi.org/10.18434/T47C7Z, 2002.

Karl, T., Guenther, A., Turnipseed, A., Tyndall, G., Artaxo, P., and Martin, S.: Rapid formation of isoprene photo-oxidation products observed in Amazonia, Atmospheric Chemistry and Physics, 9, 7753–7767, https://doi.org/10.5194/acp-9-7753-2009, 2009.

Kim, S., Karl, T., Guenther, A., Tyndall, G., Orlando, J., Harley, P., Rasmussen, R., and Apel, E.: Emissions and ambient distributions of Biogenic Volatile Organic Compounds (BVOC) in a ponderosa pine ecosystem: interpretation of PTR-MS mass spectra, Atmospheric Chemistry and Physics, 10, 1759–1771, https://doi.org/10.5194/acp-10-1759-2010, 2010.

Lindinger, W., Hansel, A., and Jordan, A.: On-line monitoring of volatile organic compounds at pptv levels by means of proton-transfer-reaction mass spectrometry (PTR-MS) medical applications, food control and environmental research, International Journal of Mass Spectrometry and Ion Processes, 173, 191–241, https://doi.org/10.1016/S0168-1176(97)00281-4, 1998.

Meurs, J., Sakkoula, E., and Cristescu, S. M.: Real-Time Non-Invasive Monitoring of Short-Chain Fatty Acids in Exhaled Breath, Frontiers in Chemistry, 10, 853 541, https://doi.org/10.3389/fchem.2022.853541, 2022.

Miller, K. J. and Savchik, J.: A new empirical method to calculate average molecular polarizabilities, Journal of the American Chemical Society, 101, 7206–7213, https://doi.org/10.1021/ja00518a014, 1979.

Müller, M., Mikoviny, T., Jud, W., D'Anna, B., and Wisthaler, A.: A new software tool for the analysis of high resolution PTR-TOF mass spectra, Chemometrics and Intelligent Laboratory Systems, 127, 158–165, https://doi.org/https://doi.org/10.1016/j.chemolab.2013.06.011, 2013.

Pagonis, D., Sekimoto, K., and de Gouw, J.: A Library of Proton-Transfer Reactions of H_3O^+ Ions Used for Trace Gas Detection, Journal of the American Society for Mass Spectrometry, 30, 1330–1335, https://doi.org/10.1007/s13361-019-02209-3, 2019.

Peltola, O., Aslan, T., Ibrom, A., Nemitz, E., Rannik, U., and Mammarella, I.: The high-frequency response correction of eddy covariance fluxes - Part 1: An experimental approach and its interdependence with the time-lag estimation, Atmospheric Measurement Techniques, 14, 5071–5088, https://doi.org/10.5194/amt-14-5071-2021, 2021.

Pfannerstill, E. Y., Reijrink, N. G., Edtbauer, A., Ringsdorf, A., Zannoni, N., Araújo, A., Ditas, F., Holanda, B. A., Sá, M. O., Tsokankunku, A., Walter, D., Wolff, S., Lavrič, J. V., Pöhlker, C., Sörgel, M., and Williams, J.: Total OH reactivity over the Amazon rainforest: variability with temperature, wind, rain, altitude, time of day, season, and an overall budget closure, Atmospheric Chemistry and Physics, 21, 6231–6256, https://doi.org/10.5194/acp-21-6231-2021, 2021.

Salthammer, T., Hohm, U., Stahn, M., and Grimme, S.: Proton-transfer rate constants for the determination of organic indoor air pollutants by online mass spectrometry, RSC Advances, 13, 17 856–17 868, https://doi.org/10.1039/D3RA01705B, 2023.

Schallhart, S., Rantala, P., Kajos, M. K., Aalto, J., Mammarella, I., Ruuskanen, T. M., and Kulmala, M.: Temporal variation of VOC fluxes measured with PTR-TOF above a boreal forest, Atmospheric Chemistry and Physics, 18, 815–832, https://doi.org/10.5194/acp-18-815-2018, 2018.

Schoon, N., Amelynck, C., Vereecken, L., and Arijs, E.: A selected ion flow tube study of the reactions of H3O+, NO+ and O2+ with a series of monoterpenes, International Journal of Mass Spectrometry, 229, 231–240, https://doi.org/10.1016/S1387-3806(03)00343-9, 2003.

Schoon, N., Amelynck, C., Vereecken, L., Coeckelberghs, H., and Arijs, E.: A selected ion flow tube study of the reactions of H3O+, NO+ and O2+ with some monoterpene oxidation products, International Journal of Mass Spectrometry, 239, 7–16, https://doi.org/10.1016/j.ijms.2004.09.003, 2004.

Schoon, N., Amelynck, C., Debie, E., Bultinck, P., and Arijs, E.: A selected ion flow tube study of the reactions of H3O+, NO+ and O2+ with a series of C5, C6 and C8 unsaturated biogenic alcohols, International Journal of Mass Spectrometry, 263, 127–136, https://doi.org/10.1016/j.ijms.2007.01.007, 2007.

Sekimoto, K., Li, S.-M., Yuan, B., Koss, A., Coggon, M., Warneke, C., and de Gouw, J.: Calculation of the sensitivity of proton-transfer-reaction mass spectrometry (PTR-MS) for organic trace gases using molecular properties, International Journal of Mass Spectrometry, 421, 71–94, https://doi.org/10.1016/j.ijms.2017.04.006, 2017.

Simon, L., Gros, V., Petit, J.-E., Truong, F., Sarda-Estève, R., Kalalian, C., Baudic, A., Marchand, C., and Favez, O.: Two years of volatile organic compound online in situ measurements at the Site Instrumental de Recherche par Télédétection Atmosphérique (Paris region, France) using proton-transfer-reaction mass spectrometry, Earth System Science Data, 15, 1947–1968, https://doi.org/10.5194/essd-15-1947-2023, 2023.

Smith, D., Chippendale, T. W., and Španěl, P.: Selected ion flow tube, SIFT, studies of the reactions of H3O+, NO+ and O2+ with some biologically active isobaric compounds in preparation for SIFT-MS analyses, International Journal of Mass Spectrometry, 303, 81–89, https://doi.org/10.1016/j.ijms.2011.01.005, 2011.

Sovová, K., Dryahina, K., and Španěl, P.: Selected ion flow tube (SIFT) studies of the reactions of H3O+, NO+ and O2+ with six volatile phytogenic esters, International Journal of Mass Spectrometry, 300, 31–38, https://doi.org/10.1016/j.ijms.2010.11.021, 2011.

Su, T.: Parametrization of kinetic energy dependences of ion–polar molecule collision rate constants by trajectory calculations, The Journal of Chemical Physics, 100, 4703–4703, https://doi.org/10.1063/1.466255, 1994.

Tani, A., Hayward, S., and Hewitt, C.: Measurement of monoterpenes and related compounds by proton transfer reaction-mass spectrometry (PTR-MS), International Journal of Mass Spectrometry, 223-224, 561–578, https://doi.org/10.1016/S1387-3806(02)00880-1, 2003.

Wang, T., Španěl, P., and Smith, D.: A selected ion flow tube, SIFT, study of the reactions of H3O+, NO+ and O2+ ions with several N- and O-containing heterocyclic compounds in support of SIFT-MS, International Journal of Mass Spectrometry, 237, 167–174, https://doi.org/10.1016/j.ijms.2004.07.009, 2004a.

Wang, T., Španěl, P., and Smith, D.: A selected ion flow tube study of the reactions of H3O+, NO+ and O2+• with some phenols, phenyl alcohols and cyclic carbonyl compounds in support of SIFT-MS and PTR-MS, International Journal of Mass Spectrometry, 239, 139–146, https://doi.org/10.1016/j.ijms.2004.07.022, 2004b.

Warneke, C., De Gouw, J. A., Kuster, W. C., Goldan, P. D., and Fall, R.: Validation of Atmospheric VOC Measurements by Proton-Transfer- Reaction Mass Spectrometry Using a Gas-Chromatographic Preseparation Method, Environmental Science & Technology, 37, 2494–2501, https://doi.org/10.1021/es026266i, 2003.

Wisthaler, A., Jensen, N., Winterhalter, R., Lindinger, W., and Hjorth, J.: Measurements of acetone and other gas phase product yields from the OH-initiated oxidation of terpenes by proton-transfer-reaction mass spectrometry (PTR-MS), Atmospheric Environment, 35, 6181–6191, https://doi.org/10.1016/S1352-2310(01)00385-5, 2001.

Yáñez-Serrano, A., Filella, I., LLusià, J., Gargallo-Garriga, A., Granda, V., Bourtsoukidis, E., Williams, J., Seco, R., Cappellin, L., Werner, C., de Gouw, J., and Peñuelas, J.: GLOVOCS - Master compound assignment guide for proton transfer reaction mass spectrometry users, Atmospheric Environment, 244, 117 929, https://doi.org/10.1016/j.atmosenv.2020.117929, 2021.

Španěl, P. and Smith, D.: SIFT studies of the reactions of H3O+, NO+ and O+2 with a series of volatile carboxylic acids and esters, International Journal of Mass Spectrometry and Ion Processes, 172, 137–147, https://doi.org/10.1016/S0168-1176(97)00246-2, 1998.

Španěl, P., Pavlik, M., and Smith, D.: Reactions of H3O+ and OH ions with some organic molecules; applications to trace gas analysis in air, International Journal of Mass Spectrometry and Ion Processes, 145, 177–186, https://doi.org/10.1016/0168-1176(95)04164-G, 1995.

Španěl, P., Ji, Y., and Smith, D.: SIFT studies of the reactions of H3O+, NO+ and O2+ with a series of aldehydes and ketones, International Journal of Mass Spectrometry and Ion Processes, 165-166, 25–37, https://doi.org/10.1016/S0168-1176(97)00166-3, 1997.

Španěl, P., Doren, J. M., and Smith, D.: A selected ion flow tube study of the reactions of H3O+, NO+, and O2+ with saturated and unsaturated aldehydes and subsequent hydration of the product ions, International Journal of Mass Spectrometry, 213, 163–176, https://doi.org/10.1016/S1387-3806(01)00531-0, 2002a.

Španěl, P., Wang, T., and Smith, D.: A selected ion flow tube, SIFT, study of the reactions of H3O+, NO+ and O2+ ions with a series of diols, International Journal of Mass Spectrometry, 218, 227–236, https://doi.org/10.1016/S1387-3806(02)00724-8, 2002b.

Španěl, P., Diskin, A., Wang, T., and Smith, D.: A SIFT study of the reactions of H3O+, NO+ and O2+ with hydrogen peroxide and peroxyacetic acid, International Journal of Mass Spectrometry, 228, 269–283, https://doi.org/10.1016/S1387-3806(03)00214-8, 2003.